

56 letters title:

Multi-Step reactions on Nuclei at High Energy

S O M M A I R E

Interactions Multiples de Particules de Hautes Energies dans les Noyaux.

Gregor v. Bochmann

Thèse de doctorat

Département de Physique

McGill University

A partir d'un modèle optique à canaux couplés, nous avons étudié l'importance des réactions de productions multiples pour les interactions cohérentes et incohérentes sur les noyaux. Des expressions analytiques sont données pour la section efficace dans les limites d'énergie infinie et de basses énergies.

Des calculs détaillés sont faits pour le système couplé de $\pi - A_1 - A_3$. Les réactions de photons avec les noyaux sont discutées dans le cadre du modèle VMD ("vector meson dominance"). Les calculs présentés sont comparés à des expériences de photo-production de ρ^0 et π^+ et de mesure de section efficace totale des photons sur des noyaux. A cette occasion, la possibilité de modifier légèrement le modèle VMD est considérée. Nous avons calculé et comparé avec les données expérimentales, la section efficace totale de neutrons sur des noyaux. Nous avons aussi discuté l'importance de la contribution des états N^* intermédiaires à l'amplitude élastique de diffusion.

Finalement, nous avons décrit comment les corrélations des fonctions d'ondes nucléaires affectent la diffusion élastique et inélastique aux hautes énergies. Nous avons aussi indiqué comment ces résultats peuvent être appliqués pour les calculs de réactions de production cohérente et incohérente.

ABSTRACT

Multi-Step Reactions of Particles on Nuclei
at High EnergyGregor v. Bochmann
Department of PhysicsPh D Thesis
McGill University

A coupled channel optical model is used to investigate the importance of multiple production steps for coherent and incoherent reactions on nuclei. Analytic expressions for the cross section are given in the low and infinite energy limit.

Detailed calculations are done for a coupled π - A_1 - A_3 system. For photo-reactions on nuclei, calculations are presented within the framework of vector dominance, and are compared with experiments of incoherent ρ^0 and π^+ photo-production and photon-nucleus total cross sections. The question of the validity of vector dominance is discussed. The total neutron cross section on nuclei is calculated and compared with experiment. The possible contribution of intermediate N^* states to the elastic scattering amplitude is also discussed.

The effects of correlations in the nuclear wave functions on elastic and inelastic scattering at high energy are described. It is indicated how these results can be used to calculate coherent and incoherent production processes.

MULTI-STEP REACTIONS OF PARTICLES ON NUCLEI
AT HIGH ENERGY

by

Gregor v. Bochmann

A thesis submitted to the Faculty of
Graduate Studies and Research in partial
fulfilment of the requirements for the
degree of Doctor of Philosophy

Department of Physics
McGill University
Montreal, P.Q.
Canada.

March 1971

© Gregor v. Bochmann 1972

ABSTRACT

Multi-Step Reactions of Particles on Nuclei
at High EnergyGregor v. Bochmann
Department of PhysicsPh D Thesis
McGill University

A coupled channel optical model is used to investigate the importance of multiple production steps for coherent and incoherent reactions on nuclei. Analytic expressions for the cross section are given in the low and infinite energy limit.

Detailed calculations are done for a coupled π - A_1 - A_3 system. For photo-reactions on nuclei, calculations are presented within the framework of vector dominance, and are compared with experiments of incoherent ρ^0 and π^+ photo-production and photon-nucleus total cross sections. The question of the validity of vector dominance is discussed. The total neutron cross section on nuclei is calculated and compared with experiment. The possible contribution of intermediate N^* states to the elastic scattering amplitude is also discussed.

The effects of correlations in the nuclear wave functions on elastic and inelastic scattering at high energy are described. It is indicated how these results can be used to calculate coherent and incoherent production processes.

PREFACE

This thesis combines work that has been done during the last two years on several problems that are important in connection with multi-step reactions on nuclei. I would like to express my gratitude to Professor B. Margolis for interesting me in this field and for his constant guidance and sound advice. Part of the work presented has been done in collaboration with my colleague, Dr. C.L. Tang, to whom I am grateful for many fruitful discussions. Similarly, I would like to acknowledge many stimulating conversations I have had with other members of the McGill Physics Department, in particular with Professor A.P. Contogouris, Dr. M. Best, Dr. T.J. Weare, and Dr. A. van Ginneken.

My work benefitted from summer visits to CERN in Geneva and to DESY in Hamburg, the Director of which I wish to thank for the hospitality extended to me.

I also wish to thank Professor S.C.C. Ting, Professor H. Meyer, and Professor H. Schopper for communicating experimental results before publication, and Professor O. Kofoed-Hansen, Professor K. Gottfried, and Dr. U. Becker for fruitful discussions.

I would finally like to thank the National Research Council of Canada for financial support, and the McGill Physics Department for awarding me the Dow-Hickson scholarship.

TABLE OF CONTENTS

	Page
ABSTRACT	i
PREFACE	ii
TABLE OF CONTENTS	iii
CHAPTER	
1. Introduction	1
2. Theory of multi-step reactions	3
2.1 The optical model for high energy reactions on nuclei	3
2.2 The multi-channel optical model	4
2.3 The solution of the optical model equation	8
2.4 Incoherent processes	13
2.5 Approximations and possible improvements	16
2.6 Some cases where multi-step processes are important	19
2.7 Infinite and low energy limits	20
3. Uncertainties of the nuclear shape and the two-body amplitudes	24
3.1 Nuclear parameters	24
3.2 The two-body interaction amplitudes	25
3.3 The definition of a closed system of channels	27
4. Applications to particular reactions	28
4.1 The π - A_1 - A_3 system	28
4.1.1. Coherent production	28
4.1.2. Incoherent production	32
4.1.3. Discussion	34

	Page
4.2 Photo-reactions and vector dominance	35
4.2.1. The vector dominance model for reactions on nuclei	35
4.2.2. The determination of the two-body amplitudes	38
4.2.3. Incoherent ρ^0 photo-production	40
4.2.4. Incoherent π^+ photo-production	43
4.2.5. Photon-nucleus total cross sections	46
4.2.6. Some difficulties of VMD and the assumption of mass dependent amplitudes	47
4.3 Neutron-nucleus total cross sections	52
5. Nuclear correlations	56
5.1 Introduction	56
5.2 The definition of the correlation function	58
5.3 Elastic scattering	60
5.4 Summed cross section for elastic and inelastic scattering	66
5.5 Discussion	73
6. Conclusions	77
REFERENCES	80
TABLES	86
FIGURE CAPTIONS	94
FIGURES	99

1. INTRODUCTION

High energy reactions on nuclei are interesting for several reasons. On the one hand, we can get information about the nuclear structure; for example, we can determine the proton or neutron distribution in the nucleus, or study the nature of nuclear correlations. On the other hand, we can get information about the interaction properties of the particles that react with the nucleus. In this connection there are two characteristics that distinguish reactions on nuclei from reactions on nucleons. These are the following:

- (a) The nuclear coherence, which produces a forward peak in the differential cross section of any diffractive reaction thus enhancing the cross section appreciably;
- (b) Processes with several reaction steps on different nucleons inside the same nucleus.

The point (b) has been used to determine the total cross section of resonances on nucleons by observing reactions where the resonance is produced on one nucleon and scattered or absorbed on another nucleon inside the same nucleus. At high energy, even a very short-lived resonance like the ρ^0 meson has a mean free path which is large compared to the nuclear radius.

When we speak of multi-step reactions in this work, we mean reactions with several production steps which could be either

transitions between different resonance channels, such as between pion, A_1 , and A_3 mesons, or the production of a resonance which transforms back to the original particle in a second production step. The presence of elastic scattering and absorption is always assumed implicitly. Most theoretical work for reactions on nuclei has been done for the cases of scattering or one-step production by using an optical model ⁽¹⁾ or the Glauber multiple scattering formalism ⁽¹⁾. However, two-step contributions to the reaction amplitude have been found to be important for the photon-nucleus total cross section ⁽²⁾ and some other reactions.

We have developed a general formalism ⁽³⁾ that allows for any number of production and transition steps between several channels. This multi-channel optical model for coherent processes is presented in chapter 2, together with a description for incoherent production reactions. In chapter 3 we point out how the parameters of the model can be determined from experiment, and we discuss the uncertainties that are involved. We have written a computer programme to be used for numerical evaluation of the multi-channel optical model. In chapter 4 we present calculations ⁽³⁾ for coherent and incoherent A_1 and A_3 meson production by pions on nuclei, a comparison between experiments and theoretical calculations ^(4, 5) for photo-reactions on nuclei, and a discussion ⁽⁶⁾ of the importance of two-step contributions by intermediate N^* states to the neutron-nucleus total cross section. Finally, in chapter 5, we discuss the effect of nuclear correlations on high energy cross sections ⁽⁷⁾.

2. THEORY OF MULTI-STEP REACTIONS

2.1 The optical model for high energy reactions on nuclei.

We consider high energy reactions of an incident particle on a nucleus. The outgoing channel, except for the nucleus, is either identical to the incident particle (scattering) or is a different particle or resonance (production reaction). We represent the incident and outgoing channels by their respective quantum numbers. We expect a diffractive two-body reaction if the spin-parity quantum numbers of the incident and outgoing channels satisfy the Gribov-Morrison relation (8)

$$P_{out} = P_{in} (-)^{S_{in} - S_{out}}$$

and the other quantum numbers remain unchanged. In this case the differential cross section for the reaction on a nucleus shows a forward peak due to the coherence of the amplitudes originating from different nucleons inside the nucleus. Experimentally, nuclear coherence at high energy has been observed for elastic scattering (9), vector meson photo-production (10), A_1 -meson production by pions (11, 12), K^0 regeneration (13), and some other reactions.

Glauber (1) has proposed a model to describe high energy scattering on nuclei which is based on the assumption that the phase shift for scattering of a particle on a nucleus is just the sum of the phase shifts for the reactions of the particle with each of the

individual nucleons inside the target nucleus. At high energy, the Fermi motion of the nucleons in the target is small with respect to the incident momentum, so that during the passage of the projectile we can take the nucleons as being fixed in their positions; and the observed amplitude is an average over the positions of the nucleons in the nucleus. Glauber has shown ⁽¹⁾ that this multiple scattering model is equivalent to an optical model description with an optical potential that is determined by the nucleon density distribution and the two-body amplitudes. The differential equation of the optical model is solved by an eikonal method, which assumes straight line trajectories for the high energy particles passing through the nucleus.

Both the Glauber multiple scattering model and the optical model have been used to describe high energy scattering on nuclei ⁽⁹⁾, and have been generalized in order to describe coherent and incoherent particle production ^(14, 15). The multi-channel optical model formalism presented here lies in the same line of development and is new in that it allows for any number of coherent production steps for a given reaction.

2.2 The multi-channel optical model.

We present here a multi-channel optical model of high energy reactions on nuclei ⁽³⁾ which is suited to describe the following phenomena:

- (a) several production channels coupled coherently to the incident channel, and to one another;

- (b) contributions to the cross section by multi-step processes (see fig.1);
- (c) the effect of the longitudinal momentum transfer at finite energies due to the mass differences of the particles under consideration;
- (d) incoherent reactions involving one incoherent step and possibly further coherent steps.

We make the following approximations which are further discussed in section 2.5:

- (A) We use the eikonal approximation which is good for reactions at small angles and high energy.
- (B) If not stated otherwise, we neglect the effects of spin and isospin on the amplitudes assuming that the spin and isospin non-flip amplitudes dominate.
- (C) We use a product wave function U_I to describe the nuclear ground state $|I\rangle$ and define the single particle density function $\rho(r)$ for a nucleon in a nucleus of mass number A by

$$|U_I(r_1, \dots, r_A)|^2 = \prod_{i=1}^A \rho(r_i) \quad (2.1)$$

where r_i is the coordinate of the i^{th} nucleon.

The effect of nuclear correlations can be incorporated into the optical model by a method described in section 5.5.

(D) We make a large A approximation which is well satisfied for medium and heavy nuclei.

In the following we first write down an optical model formalism that describes coherent reactions including several diffractive production channels and multiple step contributions as represented by the diagrams of fig. 1. This includes, in particular, the effect of the intermediate states on the elastic scattering cross section (2, 6, 16) and the effect of coupling between two diffractively produced states on their respective cross section (3). The effect of damping inside the nucleus is always included in our calculation by the presence of the imaginary part of the elastic two-body scattering amplitude.

We consider several channels α (ingoing and outgoing ones) which are described by the wave functions $\psi_\alpha(r)$. We suppose that we know all two-body amplitudes $f_{\alpha\alpha'}(k_{\alpha'})$ which are the amplitudes for producing channel α' in a reaction of the incident channel α with a single nucleon. The quantity $k_{\alpha'}$ is the momentum of the outgoing channel. For $\alpha = \alpha'$, $f_{\alpha\alpha}(k_\alpha)$ is the elastic scattering amplitude of the channel α from a nucleon.

The reaction of these channels with the nucleus and with one another is described by an optical model (17). The coherent production and scattering of the channel α inside the nucleus is described by the wave equation

$$(\nabla^2 + p_\alpha^2) \psi_\alpha(r) = \sum_{\alpha'} U_{\alpha'\alpha}(r) \psi_{\alpha'}(r) \quad (2.2)$$

which is a coupled differential equation of optical model form. The quantity $p_\alpha = \sqrt{E^2 - m_\alpha^2}$ is the magnitude of the three-momentum in the lab frame of the channel α with mass m_α , where E is the total energy of the incident particle.

The optical potentials in the above equation are of two kinds:

- (i) $U_{\alpha\alpha}(r)$ which gives rise to elastic scattering and damping for the channel α ;
- (ii) $U_{\alpha\alpha'}(r)$ with $\alpha \neq \alpha'$ which gives rise to production of channel α' by the presence of channel α .

These potentials are proportional to the corresponding two-body amplitudes $f_{\alpha\alpha'}$. Taking into account the range of the two-body interaction, the optical potentials $U_{\alpha\alpha'}(r)$ are given by

$$U_{\alpha\alpha'}(r) = -2ipA \int d^2b' \rho(b', z) \Gamma_{\alpha\alpha'}(b - b') \quad (2.3)$$

where the two-body profile functions $\Gamma_{\alpha\alpha'}(b)$ are defined by

$$\Gamma_{\alpha\alpha'}(b) = \frac{1}{2\pi ip} \int d^2k f_{\alpha\alpha'}(k) e^{-ik \cdot b} \quad (2.4)$$

Here, and in the following, r is a three-dimensional space vector, z is its component parallel to the beam of incident particles, and

b its two-dimensional component perpendicular to the beam. Since we consider reactions at high energy, we can sometimes neglect the difference between p_α and $p_{\alpha'}$, and simply write the factor p instead, as we have done in equations 2.3 and 2.4.

We sometimes neglect the range of the two-body interaction, given by $\Gamma_{\alpha\alpha'}(b)$, compared to the extension of the nuclear matter; that is, we assume $\rho(b', z)$ to be constant within the range of integration in equation 2.3. In this case the potentials $U_{\alpha\alpha'}(r)$ are given by

$$U_{\alpha\alpha'}(r) = -4\pi f_{\alpha\alpha'}(0) A \rho(r) \quad (2.5)$$

This approximation is further discussed in section 2.5.3.

2.3 The solution of the optical model equation.

To solve equation 2.2 we use the eikonal approximation^(1, 18); that is, we assume that the distances that characterize the potentials $U_{\alpha\alpha'}(r)$ are large compared to the particle wave length. This is fulfilled at high energy. We introduce the functions $\varphi_\alpha(r)$ by

$$\psi_\alpha(r) = e^{iP_\alpha z} \varphi_\alpha(r) \quad (2.6)$$

Substituting this into equation 2.2, yields

$$e^{i p_{\alpha} z} \left(\nabla^2 \varphi_{\alpha}(r) + 2 i p_{\alpha} \frac{\partial}{\partial z} \varphi_{\alpha}(r) \right) = \sum_{\alpha'} U_{\alpha' \alpha}(r) \psi_{\alpha'}(r) .$$

The functions $\varphi_{\alpha}(r)$ are slowly varying compared to the oscillations of the factor $e^{i p_{\alpha} z}$, since at high energies the right hand side of equation 2.2 is small compared to the term $p_{\alpha}^2 \psi_{\alpha}(r)$.

We can, therefore, neglect the term $\nabla^2 \varphi_{\alpha}(r)$ compared to

$2 i p_{\alpha} \frac{\partial}{\partial z} \varphi_{\alpha}(r)$ in the equation above and obtain the one-dimensional differential equation

$$\frac{\partial}{\partial z} \varphi_{\alpha}(r) = \frac{1}{2 i p_{\alpha}} \sum_{\alpha'} e^{i(p_{\alpha'} - p_{\alpha}) z} U_{\alpha' \alpha}(r) \varphi_{\alpha'}(r) . \quad (2.7)$$

The boundary condition for this equation is determined by the following remark: Before the reaction takes place, that is for small enough z ($z = -\infty$), only the incident channel α_{in} is present.

Thus, we have the boundary condition

$$\psi_{\alpha}(r) = e^{i p_{\alpha} z} \delta_{\alpha_{in} \alpha}$$

or

$$\text{for } z = -\infty \quad (2.8)$$

$$\varphi_{\alpha}(r) = \delta_{\alpha_{in} \alpha} .$$

Using a Greens function method ⁽¹⁸⁾, the amplitude $f(k)$ for scattering a particle in an optical potential $U(r)$ is found to be

$$f(k) = -\frac{1}{4\pi} \int d^3r e^{-ik \cdot r} U(r) \psi(r)$$

where $\psi(r)$ is the wave function of the particle. Extending this result, we find that the coherent amplitude $F_{\alpha_{in}\alpha}(k_\alpha)$ for producing (or scattering) the channel α off the nucleus by the incident channel α_{in} is given by

$$F_{\alpha_{in}\alpha}(k_\alpha) = -\frac{1}{4\pi} \int d^3r e^{-ik_\alpha \cdot r} \sum_{\alpha'} U_{\alpha'\alpha}(r) \psi_{\alpha'}(r). \quad (2.9)$$

We use the fact that in forward direction we can approximate the factor $e^{-ik_\alpha \cdot r}$ by $e^{-iq_\alpha \cdot b} e^{-ip_\alpha z}$ where q_α is the perpendicular component of the momentum transfer $k_\alpha - k_{\alpha_{in}}$.

Then with equations 2.6 and 2.7 we get

$$F_{\alpha_{in}\alpha}(k_\alpha) = -\frac{1}{4\pi} \int d^2b e^{-iq_\alpha \cdot b} \int_{-\infty}^{\infty} dz 2iP \frac{\partial}{\partial z} \varphi_\alpha(r)$$

which yields

$$F_{\alpha_{in}\alpha}(k_\alpha) = -\frac{iP}{2\pi} \int d^2b e^{-iq_\alpha \cdot b} [\varphi_\alpha(b, +\infty) - \delta_{\alpha_{in}\alpha}] \quad (2.10)$$

Once we know the functions $\varphi_\alpha(r)$ by solving equation 2.7 we therefore can easily get the coherent amplitude $F_{\alpha_{in}\alpha}(k_\alpha)$

for production (or scattering) by integrating equation 2.10.

Using the spherical symmetry of the nucleus, we get

$$F_{\alpha_{in}\alpha}(k_\alpha) = -i p \int_0^\infty B dB J_0(|q_\alpha| \cdot B) \times [\varphi_\alpha(B, +\infty) - \delta_{\alpha_{in}\alpha}] \quad (2.11)$$

where

$$J_0(x) = \frac{1}{2\pi} \int_0^{2\pi} e^{-ix \cos \lambda} d\lambda$$

is the Bessel function of order zero, and $B = |b|$ is the magnitude of the impact parameter b .

The coherent cross section for production (or scattering) is given by

$$\frac{d\sigma_{\alpha_{in}\alpha}^{(c)}}{d\Omega} = \frac{p^2}{\pi} \frac{d\sigma_{\alpha_{in}\alpha}^{(c)}}{dt} = |F_{\alpha_{in}\alpha}|^2 \quad (2.12)$$

We have considered two methods for solving the differential equation 2.7:

- (a) An analytical method for a square-well nuclear density distribution,
- (b) Numerical integration.

For a square-well density distribution, the function $\rho(r)$ is a non-zero constant for $|r|$ smaller than the nuclear radius R , and zero for $|r| > R$, and because of equation 2.5 the same holds for $U(r)$. From equations 2.7 and 2.6 we get in the region inside the

nucleus

$$\frac{\partial}{\partial z} \psi_{\alpha}(b, z) = \sum_{\alpha'} i \left\{ p_{\alpha} \delta_{\alpha\alpha'} - \frac{U_{\alpha\alpha'}(r)}{2p_{\alpha}} \right\} \psi_{\alpha'}(b, z)$$

$$= \sum_{\alpha'} i M_{\alpha\alpha'} \psi_{\alpha'}(b, z)$$

with a constant matrix $M_{\alpha\alpha'} = p_{\alpha} \delta_{\alpha\alpha'} - \frac{U_{\alpha\alpha'}}{2p_{\alpha}}$

whose off-diagonal elements are comparatively small.

A solution is

$$\psi_{\alpha}(b, z) = \left(e^{i(z-z_0)M} \right)_{\alpha\alpha'} \psi_{\alpha'}(b, z_0)$$

Using equation 2.6 and knowing that

$$\varphi_{\alpha}(B, -\infty) = \varphi_{\alpha}(B, -z_B) = \delta_{\alpha\alpha_{in}} \text{ and } \varphi_{\alpha}(B, \infty) = \varphi_{\alpha}(B, z_B)$$

where $z_B = \sqrt{R^2 - B^2}$ corresponds to the edge of the nucleus,

we get

$$\varphi_{\alpha}(B, \infty) = e^{i(p_{in} - p_{\alpha})z_B} \left(e^{2z_B M} \right)_{\alpha\alpha_{in}}$$

The term $e^{2z_B M}$ can be evaluated in a new system of mixed channels that diagonalizes the matrix M . We have not exploited this method for evaluating the functions $\varphi_{\alpha}(B, +\infty)$ because the square-well density distribution for the nucleus is not a good enough approximation.

To obtain the results discussed in chapter 4, we have written a computer programme which solves equation 2.7 numerically and then integrates equation 2.11.

2.4 Incoherent Processes

Incoherent processes are reactions that leave the nucleus in an excited state. Using the closure approximation which is explained in some detail in section 5.4, one gets an expression for the incoherent cross section which is the summed cross section for all possible excited final states of the nucleus. An incoherent process can be seen as taking place on a single nucleon inside the nucleus. Several incoherent steps^(15, 19), as shown in fig. 4, are possible for a given reaction. We present here a model which, for a given reaction, includes one incoherent step preceded and followed by coherent production steps and elastic scattering.

The nuclear excitation excludes coherence between amplitudes that originate from incoherent interactions at different places inside the nucleus. On the other hand, there can be interference of different amplitudes that have the incoherent step at the same place. This concept was proposed by Gottfried and Yennie⁽¹⁷⁾ for incoherent photo-production processes. In the case of ρ^0 photo-production, there is an interference between the two amplitudes represented by the diagrams of fig. 2a (one-step

incoherent production) and fig. 2b (coherent ρ^0 production followed by incoherent scattering) as long as the incoherent processes take place on the same nucleon. We generalize this concept ⁽³⁾ and assume interference between all multi-step amplitudes that have the incoherent process on the same nucleon. The two-step contributions are represented in fig.3. In the case of incoherent production of a diffractive channel, like ρ^0 photo-production or A_1 meson production by pions, the multi-step contributions are relatively large and, by destructive interference with the one-step process, produce an appreciable decrease of the incoherent cross section.

In order to formulate our model, we introduce the functions $\psi_\alpha(b, z, z_0, \alpha_0)$ which are eikonal solutions to the wave equation 2.2 with the boundary condition

$$\psi_\alpha(b, z, z_0, \alpha_0) = \delta_{\alpha\alpha_0} \quad \text{for} \quad z = z_0.$$

They represent a kind of transfer matrix. Now the incoherent cross section for producing the channel α by the incoming channel α_{in} on the nucleus is given by

$$\frac{d\sigma_{\alpha_{in}\alpha}^{(I)}}{d\Omega} = \int d^3r I_{\alpha_{in}\alpha}(r) \quad (2.13)$$

where $I_{\alpha_{in}\alpha}(r)$ is the contribution that is due to reactions with the incoherent step taking place at the point r . $I_{\alpha_{in}\alpha}(r)$

is proportional to the nuclear density $\rho(r)$ at the point r and is given by the interference of all possible multi-step amplitudes whose incoherent step takes place at the point r . Therefore we have

$$I_{\alpha_{in} \alpha} (b, z) = A \rho (b, z)$$

$$\times \left| \sum_{\alpha', \alpha''} \psi_{\alpha'} (b, z, -\infty, \alpha_{in}) f_{\alpha' \alpha''} (q) \psi_{\alpha} (b, +\infty, z, \alpha'') \right|^2$$

where the function $\psi_{\alpha'} (b, z, -\infty, \alpha_{in})$ is the wave function of the channel α' at the point $r = (b, z)$ produced coherently by the incident channel α_{in} . The factor $f_{\alpha' \alpha''} (q)$ describes the incoherent production (scattering) of the channel α'' by the channel α' , and the function $\psi_{\alpha} (b, +\infty, z, \alpha'')$ describes the production (scattering) of the channel α after the incoherent process.

We note that it follows from parity and time reversal invariance of the interaction together with the spherical symmetry of the nucleus, that

$$\psi_{\alpha} (b, -z, -z_0, \alpha_0) = \psi_{\alpha_0} (b, z_0, z, \alpha) .$$

Therefore we can write

$$I_{\alpha_{in} \alpha} (b, z) = A \rho (b, z)$$

(2.14)

$$\times \left| \sum_{\alpha', \alpha''} \psi_{\alpha'} (b, z, -\infty, \alpha_{in}) f_{\alpha' \alpha''} (q) \psi_{\alpha''} (b, -z, -\infty, \alpha) \right|^2$$

We have evaluated the incoherent cross section numerically by means of equations 2.13 and 2.14. The functions $\psi_{\alpha'} (b, z, -\infty, \alpha)$ are

obtained in the same way as the wave functions $\psi_{\alpha}(r)$ from the solution of equations 2.7 and 2.6.

It is to be noted that the channels α' and α'' in equation 2.14 are intermediate channels. The channels α' that appear in the summation are diffractively connected to the incoming channel α_{in} , whereas the channels α'' are connected to the outgoing channel α . There are two possible cases:

- (a) in- and outgoing channels are diffractively connected (example: incoherent ρ^0 photo-production). Then the channels α' and α'' belong to the same set of diffractive channels.
- (b) in- and outgoing channels are not diffractively connected (example: π^+ photo-production). Then the channels α' and α'' belong to two different exclusive sets of channels.

2.5 Approximations and possible improvements.

In deriving the above formalism for multi-step reactions on nuclei, we have made a number of assumptions. We mention here the most important ones in order to show the limits within which the present formalism can be applied without modification.

2.5.1. The eikonal approximation

The eikonal approximation (1, 18) which is used to arrive

at equation 2.7 is characterized by the condition $U(r) \ll p^2$, which is easily satisfied at high energies, and by the condition $q^2 \ll p \cdot \frac{1}{R}$, which is satisfied near the forward direction. The eikonal solution of the optical model is equivalent to the Glauber multiple scattering description (1).

2.5.2. Spin and Isospin

We assume that all amplitudes are spin and isospin independent. There is experimental evidence (10, 20) that this is fairly well satisfied for diffractive reactions.

2.5.3. The two-body interaction range

The range of the two-body interaction, which is represented by the two-body profile function $\Gamma(b)$ of equation 2.4, enters the calculation for coherent reactions in equation 2.3. The effect of the range on incoherent reactions is described by C.L. Tang in reference (21). Since the interaction range is small compared to the nuclear radius, this effect is small and can be taken into account by using an effective nuclear density function, like the one defined by equation 5.8. As long as the nuclear density distribution is not well known, these questions are more or less academic in nature.

2.5.4. Nuclear Correlations

In the model described above we have ignored the nuclear

correlations by assuming for the nucleus the product density distribution given by equation 2.1. The effects of nuclear correlations on the cross sections are described in chapter 5. Here, we mention that for coherent reactions, the correlations give rise to an effective increase by a few per cent of all the two-body amplitudes involved. For incoherent reactions there is, in addition, some t -dependent correlation contribution to the cross section which produces a forward dip in the incoherent cross section. For diffractive reactions, however, this dip is hardly seen because of the large forward coherent peak.

2.5.5. Multiple incoherent steps

In the model described above, we include any number of coherent steps, but only one incoherent step (incoherent production or incoherent scattering). The contribution of multiple incoherent steps to the incoherent cross section in the forward direction is usually of the order of 10%. In the case of π^+ photo-production, discussed in section 4.2.4, we have evaluated the incoherent two-step contribution. More details for the case of scattering are given in references (15) and (19).

2.5.6. 1/A corrections

The correspondence between the optical model description and the Glauber multiple scattering expansion ⁽¹⁾ holds only if one ignores terms of the order of $1/A$, which means it holds for heavy

nuclei. The terms of the order $1/A$ are evaluated in chapter 5 for the case of elastic scattering (see equations 5.17 and 5.33). On the other hand, the center of mass constraint ^(55, 57) of the nucleus gives rise to corrections too, which are proportional to $1/A$, and can usually be neglected.

2.6 Some cases where multi-step processes are important.

Since the two-body production amplitudes at high energies are much smaller - by a factor of 0.3 for a relatively strong diffractive production reaction - than the elastic amplitudes, which give rise to damping, the contribution of multi-step processes to the cross section is, in most cases, comparatively small if not negligible. However, there are reactions where the contributions to the cross section from one- and two-step processes are of the same order of magnitude. These are the following:

2.6.1. Photo-reactions (see section 4.2)

The vector meson dominance (VMD) model assumes that the photo-production of the final channel goes via a virtual vector meson ρ^0 , ω , or ϕ . This is a one-step process. If the reaction takes place on a nucleus, there can be real production of a vector meson with subsequent production of the final channel, which is a two-step process. The VMD model implies that one- and two-step processes are of similar strength.

2.6.2. Incoherent production of a diffractive channel

(see section 4.1.2)

In this case, the one- and two-step processes of fig. 3a, b, and c are comparable in strength because the additional step is a scattering step which has a strong two-body amplitude.

2.6.3. Reactions where the one-step process is relatively small

In this case, multi-step processes may be important or even dominating. We note the following examples:

- (i) double charge exchange reactions⁽²²⁾
- (ii) production of diffractive channels with higher mass (see section 4.1.1).

2.7 Infinite and low energy limits.

2.7.1. Coherent production

The energy dependence of the coherent production cross section on nuclei^(14, 15), ignoring the variation of the two-body amplitude, is determined by the longitudinal momentum transfer $\Delta p = (m_{out}^2 - m_{in}^2) / 2p$. In the low energy limit, that is when $\Delta p \cdot R \gg 1$ with R being the nuclear radius, the momentum difference between in- and outgoing waves destroys the equal phase relation: there is no coherent production.

In the infinite energy limit, when $\Delta p \cdot R \ll 1$, the effect of longitudinal momentum transfer can be neglected. We have maximum coherent production. If we consider one-step production processes only, and assume pure imaginary elastic amplitudes, we can use the result obtained by K.S. Kolbig and B. Margolis in ref.(15). For producing the channel α_2 by the incident channel α_1 on a nucleus, they find the forward coherent production amplitude

$$F_{\alpha_1, \alpha_2}(0) = f_{\alpha_1, \alpha_2}(0) N\left(\frac{\sigma_1}{2}, \frac{\sigma_2}{2}\right) \quad (2.15)$$

with the effective number $N(\sigma_1, \sigma_2)$ defined by

$$N(\sigma_1, \sigma_2) = \frac{1}{\sigma_2 - \sigma_1} \int d^2b \left\{ e^{-\sigma_1 T(b)} - e^{-\sigma_2 T(b)} \right\} \quad (2.16)$$

and

$$T(b) = A \int dz \rho(b, z) \quad (2.17)$$

The quantities σ_1 and σ_2 are the total cross sections on a nucleon for the channels α_1 and α_2 . For equal total cross sections $\sigma_1 = \sigma_2$ this leads to

$$F_{\alpha_1, \alpha_2}(0) = f_{\alpha_1, \alpha_2}(0) N_1\left(\frac{\sigma_1}{2}\right) \quad (2.15a)$$

where $N_1(\sigma)$ is defined by equation 2.21.

2.7.2. Incoherent production

The incoherent production cross section in the low energy limit contains no contribution from diagrams of the kind of fig. 3b to 3e, because the coherent production steps are inhibited by longitudinal momentum considerations. Ignoring multiple incoherent steps, we quote the result for one-step incoherent production obtained by K.S. Kolbig and B. Margolis in ref. (15). The incoherent production cross section can be written in the form

$$\frac{d\sigma_{\alpha, \alpha_2}^{(I)}}{d\Omega}(q) = |f_{\alpha, \alpha_2}(q)|^2 N_{eff} \quad (2.18)$$

with $N_{eff} = N(\sigma_1, \sigma_2)$.

We note that for $\sigma_1 = \sigma_2$ we have

$$N_{eff} = N_1(\sigma_1) \quad (2.19)$$

where $N_1(\sigma)$ is defined by equation 2.21.

In the infinite energy limit the situation is more complicated. Coherent production steps, followed or preceded by incoherent steps (fig. 3b through 3e) can contribute to the incoherent cross section. We refer to the sections 4.1.2, 4.2.3, and 4.2.4 as examples.

We have derived a formula for the infinite energy limit of the cross section for incoherent production of a diffractive

channel. In this case the diagrams of fig. 3b and c make an appreciable contribution to the cross section. If the total cross sections σ_1 and σ_2 are equal ($\sigma_1 = \sigma_2 = \sigma$), we have

$$N_{\text{eff}} = N_1(\sigma) - 2 N_2(\sigma) + 3/2 N_3(\sigma) \quad (2.20)$$

where the effective numbers $N_m(\sigma)$ are defined by

$$N_m(\sigma) = \frac{1}{m!} \frac{1}{\sigma} \int d^2b (\sigma T(b))^m e^{-\sigma T(b)} \quad (2.21)$$

It is interesting to note that we can derive this result both from the optical model presented above, and from the multiple scattering formalism ⁽¹⁵⁾. The multi-step contributions corresponding to the diagrams of fig. 3b and c are contained in what the authors of reference (15) call the semi-coherent cross section.

3. UNCERTAINTY OF THE NUCLEAR SHAPE AND THE TWO-BODY AMPLITUDES

3.1 Nuclear parameters.

For calculations of high energy cross sections on nuclei it is important to know the density distribution of the nucleons inside the target nucleus. In this work we are mostly interested in reactions on medium and heavy nuclei. We describe the nuclear state by a product wave function with an average density distribution $\rho(r)$ defined in equation 2.1, and which represents the average over all individual nucleon wave functions and ignores the correlations between nucleons. We show in chapter 5 how the effect of nuclear correlations on the cross sections can be evaluated.

There are a number of methods to determine the nuclear density distributions. We mention here the following:

- (a) electron scattering experiments,
- (b) mesonic atoms,
- (c) high energy reactions on nuclei.

In order to get a consistent picture between different methods of measurement, one usually assumes a certain parameterization of the density distribution $\rho(r)$. Throughout this work, all numerical calculations have been done with the Wood-Saxon density function ⁽²³⁾

$$\rho(r) = \rho_0 \left\{ 1 + e^{(r-R)/c} \right\}^{-1} \quad (3.1)$$

with a normalization constant ρ_0 .

We have the following two free parameters:

- (i) the radius R ,
- (ii) the parameter c for the surface thickness.

We have usually taken the value $c = 0.545$ fm from electron scattering experiments ⁽²⁴⁾. For the parameter R , we make use of its A dependence in the form

$$R = R_0 A^{1/3} \quad (3.2)$$

where the value of R_0 is determined from experiments.

In theoretical calculations of cross sections on nuclei, we often ignore the effect of nuclear correlations and of the two-body interaction range. For a comparison with experiments we therefore should use an effective density distribution where these effects are "folded in", as is done in equation 2.3 or 5.8 and 5.35. On the other hand, one can analyse the experimental data, ignoring the interaction range and correlations, in order to get the effective nuclear density distribution directly. Such a determination of the radius R is done from the data of coherent ρ^0 photo-production ⁽²⁵⁾ and yields the values of R listed in Table 1. The average, over all measured nuclei, yields $R_0 = (1.12 \pm 0.02)$ fm.

3.2 The two-body interaction amplitudes.

There are two kinds of two-body amplitudes that enter

our calculations:

- (a) amplitudes that, in principle, can be directly measured by two-body reaction experiments, such as $f(\gamma N \rightarrow \rho^0 N)$, or $f(\rho N \rightarrow \pi N)$ which is determined from the time reversed reaction $\pi N \rightarrow \rho N$.
- (b) amplitudes that cannot be directly measured because both, incoming and outgoing channels, are resonances. Such are the amplitudes for elastic scattering of resonances, like $\rho N \rightarrow \rho N$, or for a production like $A_1 N \rightarrow A_3 N$.

The amplitudes of the kind (b) can, in principle, be determined from reactions on nuclei, as has been done for the imaginary part of the elastic scattering amplitude — related to the total cross section — of the resonances $\rho^0(765)$ (26, 27), $\phi(1019)$ (28), $A_1(1070)$ (12, 16) and the Q enhancement $Q(1300)$ (29). On the other hand, theoretical models for strong interactions may often give estimates for the amplitudes of the kind (b).

There are often additional uncertainties in the two-body interactions. We mention the following ones:

- (a) the phase $\beta = \frac{\text{Re } f(q)}{\text{Im } f(q)}$ of the amplitude $f(q)$,
- (b) the importance of spin flip amplitudes,
- (c) the isospin decomposition.

However, in many cases these uncertainties can be resolved.

3.3 The definition of a closed system of channels.

In the description of multi-step reactions on nuclei, as given in equation 2.2, we have a system of channels α that are coupled to one another through the two-body amplitudes $f_{\alpha\alpha'}(q)$. Besides the incoming and outgoing ones, there are channels that play the role of intermediate real states during the interaction with the nucleus. Then the following question arises: How many intermediate channels α do we have to include in the calculation in order to get a realistic answer for the cross section? In principle, all diffractively coupled channels can contribute. There are many reactions, however, where the contribution from intermediate channels is very small ⁽³⁾. In practice, uncertainties about the amplitudes and the complexity of the calculations limit the number of channels to be included in the model.

There is another interesting question, which is discussed in section 4.3: Do only diffractive resonances of the two-body interaction contribute to the multi-step reactions in the form of intermediate states, or does some "diffractive background" of the mass spectrum contribute as well?

4. APPLICATIONS TO PARTICULAR REACTIONS

4.1 The π - A_1 - A_3 system

We consider the production of the mesons A_1 (1070) and A_3 (1640) on nuclei by incident pions. The mesons probably have spin and parity 1^+ and 2^- respectively (30) and are therefore expected to be produced diffractively on nucleons. The A_1 has been seen to be produced coherently on nuclei (12, 31). We assume for present purposes that the π , A_1 and A_3 form a closed system with reference to equation 2.2, i.e. that couplings to other mesons are negligible.

4.1.1. Coherent production

One can expand the amplitude $F_{\alpha_1\alpha_2}$ on the nucleus in terms of multi-step amplitudes $F_{\alpha_1\alpha_2}^{(i)}$ where i indicates the number of production steps involved. Figure 1 shows diagrams that represent one-, two-, and three-step amplitudes. If the coupling between the channels is not too strong, the contribution of three or more steps is negligible. It is to be noted that the elastic scattering is not counted as a step.

A. The infinite energy limit

We now look at the high energy limit where the longitudinal momentum transfer can be neglected. If we assume that the elastic

scattering amplitude is the same for all channels, and if we use equations 2.7 and 2.10, we find the following expressions for the forward amplitude

$$F_{\alpha_1, \alpha_2}^{(1)}(0) = f_{\alpha_1, \alpha_2}(0) N_1\left(\frac{\sigma'}{2}\right) \quad (4.1)$$

$$F_{\alpha_1, \alpha_2}^{(2)}(0) = -\frac{f_{\alpha_1, \alpha_1'}(0) f_{\alpha_1' \alpha_2}(0)}{f_{\alpha_1' \alpha_1'}(0)} N_2\left(\frac{\sigma'}{2}\right)$$

with the effective numbers $N_m(\sigma)$ defined by equation 2.21. The quantity σ'_α is related to the total two-body cross section σ_α of the channel α and to the phase $\beta = \frac{\text{Re } f_{\alpha\alpha}(0)}{\text{Im } f_{\alpha\alpha}(0)}$ by

$$\sigma'_\alpha = \sigma_\alpha (1 - i\beta) = \frac{4\pi f_{\alpha\alpha}(0)}{ik} \quad (4.2)$$

Values for $N_1(\sigma)$ and $N_2(\sigma)$ are given in fig. 5 for the case of pure imaginary amplitudes.

The forward amplitude for A_1 production then is given by

$$F_{\pi A_1}(0) = f_{\pi A_1}(0) \left\{ N_1\left(\frac{\sigma'}{2}\right) - \frac{f_{\pi A_3}(0) f_{A_3 A_1}(0)}{f_{\pi A_1}(0) f_{A_3 A_3}(0)} N_2\left(\frac{\sigma'}{2}\right) \right\} \quad (4.3)$$

where we have neglected higher than two-step contributions.

Similarly we have for A_3 production

$$F_{\pi A_3}(0) = f_{\pi A_3}(0) \left\{ N_1\left(\frac{\sigma'}{2}\right) - \frac{f_{\pi A_1}(0) f_{A_1 A_3}(0)}{f_{\pi A_3}(0) f_{A_1 A_1}(0)} N_2\left(\frac{\sigma'}{2}\right) \right\} \quad (4.4)$$

Experimentally ⁽³⁰⁾ it is found that $f_{\pi A_3}(0) / f_{\pi A_1}(0) \approx 0.35$

and $f_{\pi A_1}(0) / f_{\pi\pi}(0) \approx 0.27$ at 8 Gev/c incident pion momentum.

We must also know $(f_{A_1 A_3} / f_{A_1 A_1})$ and $(f_{A_1 A_3} / f_{A_3 A_3})$ in order to

have a definite answer. It is reasonable to expect that these ratios will be of the same order of magnitude as $(f_{\pi A_1} / f_{\pi\pi})$.

If $(f_{A_1 A_3} / f_{A_3 A_3}) \approx (f_{\pi A_1} / f_{\pi\pi})$, the one-step process in equation

4.3, corresponding to the first term on the right hand side, is dominant for A_1 production, whereas for A_3 production both terms can be important.

It is to be noted that at finite energies the two-step process for A_1 production through the A_3 is further inhibited by longitudinal momentum transfer effects due to the higher mass of the A_3 . The same would be true for possible couplings to other high mass bosons. It is unlikely that there is any important coherent coupling to mass states lower than the A_1 (12, 31).

We have a strong indication then that one can, to good approximation, calculate A_1 production as a one-step process.

In A_3 production we are in a more complicated situation. The fact that the one-step and two-step processes are comparable means that in detailed calculations we must know, or be able to determine from the production experiments, $(f_{A_1 A_3} / f_{A_1 A_1})$ as well as $\sigma_{\text{tot}}(A_1 N)$ and $\sigma_{\text{tot}}(A_3 N)$. In principle we should be able to determine all of these from reactions on nuclei since we have the whole periodic table to work with as targets. There is, however, the real possibility that other bosons contribute as intermediate states.

B. Coherent production at finite energies.

At finite energies we do not have simple expressions like equations 4.3 and 4.4 to work with. We have solved the problem numerically as described in chapter 2. Some results for the coherent production differential cross sections on Copper are shown in figs. 6 and 7. In these calculations all two-body amplitudes are taken to be pure imaginary. We have taken the A_3 -nucleon total cross section equal to the pion-nucleon total cross section, $\sigma_\pi = 26$ mb. The A_1 -nucleon total cross section σ_{A_1} has been taken equal to $\sigma_\pi^{(12)}$ or to $1/2 \sigma_\pi^{(16)}$. The A_3 production cross section is given for different values of the parameter

$$X = \frac{f_{\pi A_1}(0) f_{A, A_3}(0)}{f_{\pi A_3}(0) f_{A, A_1}(0)} \quad (4.5)$$

which determines the relative strength of the one-step and two-step processes. For positive values of X these two processes interfere destructively (fig. 7a and 7b). However, negative values of X (fig. 7c) would occur if the production amplitude $f_{\pi A_3}(0)$ has opposite phase to $f_{\pi A_1}(0)$, which may be reasonable if one assumes that the A_3 production on a nucleon proceeds via two pomeron exchange. (Multi-pomeron exchange has been discussed by Frautschi and Margolis ⁽³²⁾ and by Jacob and Pokorski ⁽³²⁾).

Table 2 lists some coherent cross sections for A_1 and A_3 production on different nuclei and at different energies. It is

to be noted that for the values of X considered here, A_1 production differs very little from the value obtained with $X = 0$ (no coupling of A_1 to A_3). On the other hand, A_3 production is very sensitive to the value of X . For $X \approx -1$ and at energies around 15 Gev the cross section on nuclei divided by the corresponding two-body production cross section is about equal for A_3 and A_1 production. The two-body cross section is, however, about 10 times weaker for A_3 production than for A_1 production. For $X \approx 1$, A_3 production on the nucleus is very weak in the model studied here.

4.1.2 Incoherent production

We now discuss the calculation of incoherent production of A_1 and A_3 mesons using equations 2.13 and 2.14. It is to be noted (see section 2.5.4.) that this method is not expected to yield a very accurate incoherent production cross section at the smallest values of momentum transfer. However, at very small values of t , coherent production is dominant.

We write the incoherent cross section for the production of particle α by incident pions as

$$\frac{d\sigma_{\alpha}^{(I)}}{d\Omega} = |f_{\pi\alpha}(t)|^2 N_{eff} \quad (4.6)$$

where N_{eff} is an effective nucleon number for the nucleus under consideration. For A_1 production at low energies we use only the term $\alpha' = \text{pion}$ and $\alpha'' = \alpha$ in the sum on the right side of

equation 2.14, which corresponds to one-step production of α by pions. In agreement with equation 2.18 we find $N_{\text{eff}} = N(\sigma_{\pi}, \sigma_{A_1})$, the latter being defined by equation 2.16. Keeping all terms of the sum in equation 2.14 includes the following processes, which contribute to the production of the state α , and which are represented in fig.3:

fig. 3a : one-step production

fig. 3b : coherent production of α followed by incoherent scattering of α (term $\alpha'' = \alpha' = \alpha$)

fig. 3c : coherent production of α preceded by incoherent scattering of the pion (term $\alpha'' = \alpha' = \text{pion}$)

fig. 3d and 3e: two-step production, one of which is coherent

in addition: processes with more than one coherent production step.

Some values of N_{eff} are given in Table 3 for different values of the parameters of the theory. The figures 6 and 7 show incoherent as well as coherent production of A_1 and A_3 and the sum of coherent and incoherent cross sections for the parameters listed.

It is to be noted that the contribution of the multi-step processes of fig. 3b through e disappears at lower energies due to longitudinal momentum transfer which inhibits the coherent production. At high energies we have destructive interference between the one-step (fig. 3a) and the multi-step processes. The contributions from the

diagrams of fig. 3b and 3c are comparable in strength to the one-step process because the additional step is elastic scattering which has a strong amplitude. As a result, N_{eff} decreases appreciably for increasing energy. This is typical for the incoherent production of any diffractive channel. For A_1 production, as far as the influence of an intermediate A_3 state can be neglected, N_{eff} is given in the infinite energy limit by equation 2.20.

4.1.3 Discussion

It can be seen from the above that the simple one-step theory which one is familiar with for coherent and incoherent diffractive production can be in serious error. In the case of a relatively light and strongly produced boson like the A_1 meson, the one-step theory should be adequate for coherent production, whereas for the A_3 meson it is likely not. In incoherent production at energies of the order of 10 Gev or greater, the simple one-step theory needs corrections due to coherent production preceded or followed by incoherent scattering. By going to lower energies this correction may become negligible due to longitudinal momentum transfer considerations. However, since the details of the coupling strength of one unstable boson to another are unknown, it is difficult to evaluate the corrections in detail. To this end experiments on coherent and incoherent production of pion (and kaon) resonances will be very valuable. With enough data perhaps one will be able to sort out coupling strengths as well as unstable particle cross sections.

It is to be noted that, since the time when the above calculations were completed, an experiment ⁽¹²⁾ has been done that seems to throw new light on the question of the nature of the A_1 ⁽¹⁶⁾. Is it a resonance or some kinematical enhancement? This experiment yields a very broad mass distribution for the 3π system produced coherently by incident pions on nuclei. The total cross section of the 3π system on a nucleon is of the order of 23 mb at 15 Gev incident energy (see fig. 17) which is very similar to the value found for the ρ^0 meson ⁽²⁶⁾. This is consistent with what one expects for the A_1 being a resonance (unstable particle) if one uses quark model calculations. According to the simple additive quark model ⁽³³⁾ one expects the total cross sections for the A_1 and ρ meson to be the same as for the pion. The A_3 meson has not been seen to be produced on nuclei.

4.2 Photo-reactions and vector dominance

4.2.1. The vector dominance model for reactions on nuclei.

The vector meson dominance (VMD) model ⁽³⁴⁾ describes the strong interactions of photons in terms of the vector mesons $\rho^0(765)$, $\omega(784)$ and $\phi(1019)$. It connects the hadronic electro-magnetic current with the fields of the vector mesons which have the same quantum numbers as the electro-magnetic current, namely $j = 1$, $P = -1$, and $C = -1$. This connection can be made through the current

field identity

$$j_{\mu}^{\text{EM}}(x) = - \sum_{V=\rho, \omega, \phi} \frac{m_V^2}{2g_V} V_{\mu}(x) \quad (4.8)$$

where g_V are the coupling constants, m_V the masses, and $V_{\mu}(x)$ the fields of the vector mesons $V = \rho^0, \omega, \text{ and } \phi$. The assumption is made that the vector mesons ρ, ω and ϕ completely saturate the electro-magnetic current.

From equation 4.8 a relation between interaction amplitudes can be obtained:

$$f_{\gamma\alpha}(q) = \sum_{\substack{V= \\ \rho, \omega, \phi}} \sqrt{\frac{g_{\text{EM}}}{4} \left(\frac{g_V^2}{4\pi}\right)^{-1}} f_{V\alpha}(q) \quad (4.9)$$

where $f_{\gamma\alpha}$ [$f_{V\alpha}$] is the reaction amplitude for an incident photon [vector meson V] to produce the channel α on a nucleon. g_{EM} is the electromagnetic coupling constant $g_{\text{EM}} \approx \frac{1}{137}$, usually called α . Figure 8b shows the diagram that corresponds to equation 4.9. For photon elastic scattering we use the diagram of fig. 8c which gives rise to the identity

$$f_{\gamma\gamma}(q) = \sum_{\substack{V= \\ \rho, \omega, \phi}} \frac{g_{\text{EM}}}{4} \left(\frac{g_V^2}{4\pi}\right)^{-1} f_{V\gamma}(q) \quad (4.10)$$

where we have assumed that there is no coupling between the vector mesons, which means

$$f_{VV'}(q) = 0 \quad \text{for } V \neq V' \quad (4.11)$$

Now we come to photon-induced reactions on nuclei.

The vector meson channels $V = \rho^0, \omega, \text{ and } \phi$ are diffractively connected to the incoming photon γ , and are therefore produced coherently. Coherent photo-production has been discussed elsewhere^(14, 15). The concept of multi-step photo-reactions on nuclei has been developed independently by several authors. Multi-step contributions are important both for the elastic scattering of photons on nuclei (fig. 9) which is related to the photon total cross sections on nuclei⁽²⁾, and for incoherent photo-production^(4, 17) (fig. 10). In these two cases it turns out that, at high energy, the one-step and two-step amplitudes are of the same order of magnitude. For lower energy, however, the coherent production of vector mesons is suppressed by the longitudinal momentum transfer, and the two-step amplitudes (figs. 9b and 10b) vanish. The one-step amplitude which remains is characterized by (i) a very long mean free path of the photon through the nucleus due to the small value of the photon-nucleon total cross section σ_γ of the order of 0.12 mb, and (ii) by the two-body reaction amplitude described by the VMD model.

At very high energy the interference of one-step and two-step amplitudes makes the photon behave like a mixture of vector mesons. We have VMD on the nucleus as a whole, and consequently the photon nucleon total cross section appears to be of the order of 25 mb. However, it is to be noted that measured photon cross sections are much smaller due to the weak electromagnetic coupling constant g_{EM} of the photon.

4.2.2. The determination of the two-body amplitudes.

The purpose of the following investigation is to test if the VMD hypothesis together with the eikonal multi-channel formalism can explain the experimental data that are available for photo-reactions on nuclei. Therefore it is important to know the values of the two-body amplitudes that enter the calculations. In principle, there are several methods for determining these; we come back to this in the section 4.2.6. We describe here the method we have adopted to get the two-body amplitudes used in the calculations of sections 4.2.3 through 4.2.5.

A. ρ^0 photo-production.

The phase $\beta = \frac{\text{Re } f(o)}{\text{Im } f(o)}$ of the amplitude $f_{\rho\rho}$ for ρ^0 scattering on nucleons is determined through the quark model⁽³³⁾ relation

$$f(\rho^0 N \rightarrow \rho^0 N) = \frac{1}{2} \left\{ f(\pi^+ p \rightarrow \pi^+ p) + f(\pi^- p \rightarrow \pi^- p) \right\} \quad (4.12)$$

from the measured phase of the pion proton scattering amplitudes⁽³⁵⁾. There have also been direct measurements⁽³⁶⁾ of the phase β for ρ^0 photo-production, which confirm the values we have used. It is to be noted that if one accepts equation 4.9, the phase of the ρ^0 photo-production amplitude $f_{\gamma\rho}(o)$ is the same as that of $f_{\rho\rho}(o)$.

The magnitude of the amplitude $f_{\rho\rho}(o)$ and the ρ -nucleon total cross section σ_ρ , which is related to it by the optical

theorem, are determined from ρ^0 production experiments through the VMD relation

$$\frac{d\sigma}{dt}(\gamma p \rightarrow \rho^0 p)_{t=0} = \frac{1}{16} \frac{g_{EM}^2}{4\pi} \left(\frac{\gamma_p^2}{4\pi} \right)^{-1} \sigma_p^2 (1 + \beta^2) \quad (4.13)$$

which follows from equation 4.9. We have used the value $\frac{\gamma_p^2}{4\pi} = 0.5$, taken from the compilation of S.C.C. Ting (28), and the values of $\frac{d\sigma}{dt}(\gamma p \rightarrow \rho^0 p)$ from a fit to data of ρ^0 photo-production on hydrogen (37). These values and other parameters for the calculations are listed in Table 4.

It is to be noted that the values for the ρ^0 total cross section σ_ρ decreases with increasing energy. There are further indications that σ_ρ is falling with energy:

- (a) σ_γ is decreasing with energy in a similar manner at energies of several Gev (38, 39). It is to be noted that according to VMD

$$\sigma_\gamma = \frac{g_{EM}^2}{4} \sum_{V=\rho, \omega, \phi} \left(\frac{\gamma_V^2}{4\pi} \right)^{-1} \sigma_V \quad (4.14)$$

- (b) The additive quark model (33) gives

$$\sigma_\rho = \frac{1}{2} \{ \sigma_{\pi^+} + \sigma_{\pi^-} \}$$

and the π -nucleon cross sections also fall with energy at a rate similar to that deduced for σ_ρ here.

B. The amplitudes for the vector mesons ω and ϕ .

The contribution of the vector mesons ω and ϕ to the reactions discussed here is small compared to the contribution of the ρ^0 meson, mainly because their coupling to the photon is weaker. We have used for the coupling constants the values (28) $\frac{\gamma_\omega^2}{4\pi} = 4.69$ and $\frac{\gamma_\phi^2}{4\pi} = 3.04$. The ϕ -nucleon total cross section σ_ϕ is taken to be 12 mb (28). For the ω -nucleon total cross section σ_ω we use the same value as for σ_ρ (40).

We have used the same phase β for the amplitudes of all three vector mesons.

The direct coupling between different vector meson channels has been neglected (see equation 4.11). Its possible influence on the reactions discussed below is probably very small.

C. π^+ photo-production.

Within the VMD model we assume that only the ρ meson contributes significantly to the π^+ photo-production reaction. Then the π^+ photo-production amplitude has no influence on the ratio between cross sections on nuclei and on protons, which is the ratio we are interested in. The π^+ -nucleon total cross section from reference (41) is listed in Table 4.

4.2.3. Incoherent ρ^0 photo-production

A. Theory.

Gottfried and Yennie (17) describe incoherent ρ^0 production in terms of a superposition of one and two-step processes. In the

one-step process (fig. 2a) the ρ^0 meson is produced incoherently on a nucleon and then proceeds, with some damping, to be emitted from the nucleus which has been excited. The two-step process (fig. 2b) consists of coherent production on one nucleon (no nuclear excitation) followed by incoherent scattering (nuclear excitation occurs) of the ρ^0 meson on another nucleon.

We arrive at the same result ⁽⁴⁾ by using equations 2.13 and 2.14 for a system of particles consisting of the incoming photon γ and the diffractively produced ρ^0 . Because of the smallness of the electromagnetic interaction amplitude, we consider only one-step processes for coherent production. Equation 2.7 yields the wave function $\varphi_\rho(r)$ given by

$$\begin{aligned} \varphi_\rho(b, z) = & -\frac{A}{2} \sigma_\rho' \int_{-\infty}^z dz' \rho(b, z') e^{i(k_\gamma - k_\rho) z'} \\ & \times e^{-\frac{A}{2} \sigma_\rho' \int_{z'}^z dz'' \rho(b, z'')} \end{aligned} \quad (4.15)$$

The wave numbers for the photon and ρ^0 meson are k_γ and k_ρ respectively, and the quantity σ_ρ' , defined by equation 4.2, is essentially the ρ -nucleon total cross section σ_ρ .

Ignoring the very small damping of the incoming photon, equations 2.13 and 2.14 can be re-written in the form

$$\frac{d\sigma^{(I)}}{d\Omega} \equiv \frac{d\sigma^0}{d\Omega} N_{\text{eff}} = \int d^2b dz I(b, z)$$

with

$$I(b, z) = \frac{d\sigma^{\rho}}{d\Omega} A_{\rho}(b, z) e^{-A\sigma_{\rho} \int_z^{\infty} dz' \rho(b, z')} \times \left| e^{i(k_{\gamma} - k_{\rho})z} + \varphi_{\rho}(b, z) \right|^2 \quad (4.16)$$

where $\frac{d\sigma^{\rho}}{d\Omega}$ is the ρ° photo-production differential cross section on a neutron or proton (taken equal). The effective nucleon number N_{eff} is a function of A , energy, and σ_{ρ} .

At low energies around 2 Gev the one-step process dominates. The two-step process is inhibited due to mismatch of the photon and ρ° meson wave numbers because of the mass of the ρ° meson. Ignoring the real part of the amplitude one has then an incoherent production cross section

$$\frac{d\sigma^{(\tau)}}{d\Omega} = \frac{d\sigma^{\rho}}{d\Omega} N(0, \sigma_{\rho}) \quad (4.17)$$

with the effective number $N(\sigma_1, \sigma_2)$ defined in equation 2.16.

At very high energy where the mass of the ρ° is negligible, we find

$$\frac{d\sigma^{(\tau)}}{d\Omega} = \frac{d\sigma^{\rho}}{d\Omega} N(\sigma_{\rho}, \sigma_{\rho}) \quad (4.18)$$

The photon in this case behaves as though it were a ρ° meson. Since $N(\sigma_{\rho}, \sigma_{\rho})$ is considerably less than $N(0, \sigma_{\rho})$ the cross section has fallen in going from photon energies of a couple of Gev to infinite energy. At intermediate energies the cross section decreases monotonically as the calculations of references (17) and (42) show.

B. The comparison with experiments.

We have calculated⁽⁴⁾ the incoherent photo-production of ρ^0 mesons on different nuclei and for different energies. The results are shown in fig. 11 along with the available experimental data (42, 43). It is to be noted that, in contrast to what some authors have expected, we find a relatively small variation of the effective nucleon number N_{eff} with energy. This is a result of the values used for σ_ρ which are relatively small and decreasing with energy (see section 4.2.2 and Table 4). We remark that at the momentum transfer under consideration, there should be some correction due to higher order multiple step incoherent processes. We come back to this point below.

We conclude from the comparison of fig. 11 that there is no clear discrepancy between the experimental data and the theoretical predictions. However, the experimental error is sizeable.

4.2.4. Incoherent π^+ photo-production.

The calculations for incoherent π^+ photo-production on nuclei (17, 5) are very similar to those for incoherent ρ^0 production, even though the pion is not coupled coherently to the photon and ρ meson. Besides a factor Z/A , where Z is the atomic number of the nucleus, we get the same formulas as above with σ_ρ in equation 4.16 replaced by the pion-nucleon total cross section σ_π ; and $\frac{d\sigma^0}{d\Omega}$ being the π^+ photo-production differential cross section on protons. Again, we have a one-step low energy limit with

$N_{\text{eff}} = \frac{Z}{A} N(0, \sigma_{\pi})$, and an infinite energy limit with

$N_{\text{eff}} = \frac{Z}{A} N(\sigma_{\rho}, \sigma_{\pi})$, where the photon behaves like a ρ^0 meson.

In this case of π^+ photo-production we have, in addition, determined the contribution to the cross section by processes with two incoherent steps (5). Figure 4 shows the corresponding diagrams. Appropriate formulae for the case of elastic scattering have been derived in the literature (15, 19). In analogy, we find that with the assumption of equal elastic scattering amplitudes $f_{\pi\pi} = f_{\rho\rho}$ one has the following expression for the two-incoherent-step contribution in the limit of high energy, where the incoming photon acts like a vector meson:

$$\frac{d\sigma^{(\text{II})}}{d\Omega}(q) = \frac{Z}{A} \frac{d\sigma^0}{d\Omega}(q) \sum N_2(\sigma) \times \frac{\sqrt{\sigma_{\text{el}}}}{\sigma} \frac{a}{a+a_{12}} e^{\frac{a_{12}^2}{a+a_{12}} q^2}$$

In the low energy limit we have

$$\frac{d\sigma^{(\text{II})}}{d\Omega}(q) = \frac{Z}{A} \frac{d\sigma^0}{d\Omega}(q) \{ N(0, \sigma) - N_1(\sigma) \} \times \frac{\sqrt{\sigma_{\text{el}}}}{\sigma} \frac{a}{a+a_{12}} e^{\frac{a_{12}^2}{a+a_{12}} q^2}$$

where the effective numbers $N(\sigma_1, \sigma_2)$ and $N_m(\sigma)$ are defined in equations 2.16 and 2.21. Here $\sigma_{\text{el}}[\sigma]$ is the elastic [total] cross section of a pion or ρ^0 meson on a nucleon, and $a[a_{12}]$ is the slope of the elastic [production] differential cross section of the pion or ρ^0 meson respectively.

For intermediate energies we evaluate the two-step contribution to the cross section approximately by linear interpolation between these two formulae with the parameter $X = \{N_{\text{eff}} - N_1(\sigma)\} / \{N(0, \sigma) - N_1(\sigma)\}$; where $X = 0$ [$X = 1$] corresponds to the infinite [low] energy limit.

Figure 12 shows a comparison of the calculated effective number N_{eff} (including two incoherent steps) with π^+ photo-production measurements ⁽⁴⁴⁾. The normalization of the calculated cross section for every value of momentum transfer is fitted to the experimental data. This was necessary because the measured effective number $N_{\text{eff}}^{(\text{exp})}$ shows a strong t -dependence due to nuclear correlation, which is discussed in chapter 5. Thus it is the variation of N_{eff} with energy and with nuclear size that we utilize to make a comparison between theory and experiment. Figure 12 shows reasonable agreement.

We note that the contribution by processes with two incoherent steps is of the order of 15% for lead and 8% for carbon, for all values of momentum transfer considered. Again, we are interested in the A -dependence of this contribution.

A similar amount of two-step contribution is present for incoherent ρ^0 photo-production. However, the effects of correlations introduce cross section changes of the same order of magnitude in the opposite direction. In any case, it appears to us that present data does not make necessary their consideration.

4.2.5. Photon-nucleus total cross sections

Total photon-nucleus cross sections have been calculated by several groups ⁽²⁾. One calculates the forward photon-nucleus scattering amplitude using eikonal methods and then invokes the optical theorem to get the total cross section. The scattering amplitude, according to VMD, is the sum of two amplitudes (see fig. 9), the diffractive scattering amplitude, corresponding to photon scattering on each nucleon, summed over all nucleons (proportional to nucleon number A) and a two-step regenerative amplitude corresponding to photo-production of one of the vector mesons ρ , ω or ϕ on one nucleon followed by radiative capture on another nucleon. The coupling between the vector mesons ω and ϕ is neglected. The damping of the intermediate vector mesons by the target nucleons creates a shadow, which expresses itself by the fact that the total cross section $\sigma(\gamma, A)$ is not proportional to the nucleon number A .

There is now experimental data ^(38, 45) confirming the presence of this nuclear shadow. It is difficult to fit these experimental data if one assumes the ρ^0 total cross section σ_ρ is larger than 30 mb ⁽³⁸⁾. This raises the question of the validity of the VMD model in its present form. It was suggested that heavier vector mesons, so far unknown, were coupled to the photon in the same way as the vector mesons ρ , ω , and ϕ .

We have done calculations ⁽⁵⁾ for the photon-nucleus total cross sections using the parameters discussed in section 4.2.2. The

results are shown in fig. 13 (full lines) together with data from reference (38). The purpose of these calculations was to show that one can get around the assumption of additional heavy vector mesons by using realistic values for the two-body amplitudes. As in incoherent ρ^0 photo-production we note a comparatively weak energy dependence of the photon total cross sections. This is due to the decrease of σ_ρ with energy and to the presence of a non-zero real part in the ρ -nucleon forward scattering amplitude.

4.2.6. Some difficulties of VMD and the assumption of mass dependent amplitudes.

We conclude from the above calculations that VMD together with the eikonal methods used provide a reasonable description of the corresponding experiments. The experimental uncertainties are still fairly large, and it is not possible to say if any additional assumptions are necessary to describe the experimental data. However, we note some apparent difficulties:

- (a) The ratio of photon total cross sections on nuclei and nucleons respectively indicate that for heavy nuclei the calculated values are too low, as shown in fig. 13 (full lines);
- (b) The theoretical result for the effective number N_{eff} of incoherent π^+ photo-production (see fig. 12) is too low for heavy nuclei. This comes out more clearly in fig. 14, where the same data is presented in a

different way: For every value of momentum transfer and for the energies 8 and 16 Gev, the experimental and theoretical values for N_{eff} are normalised to the corresponding value for carbon;

- (c) The calculations for π^+ photo-production predict too strong an energy dependence, as already noticed by the authors of reference (44);
- (d) There are several methods to determine the ρ^0 total cross section on nucleons σ_ρ , which give slightly different results.

Besides the method described in section 4.2.2, we have determined σ_ρ from measurements of the photon-nucleon total cross section σ_γ , using equation 4.14. These values of σ_ρ are listed in Table 5. We have taken the same values for the coupling constants $\frac{\gamma_V^2}{4\pi}$ and the phase β as in section 4.2.2. The values of σ_γ are fits to the data from references (38) and (39), and are listed in Table 5. The contribution of the mesons ω and ϕ to the photon total cross section is taken to be 16% (38).

We mention a third method to determine σ_ρ which is by coherent ρ^0 photo-production experiments on nuclei (26, 27). The final results of these experiments have been summarized by D.W.G.S. Leith in reference (10).

The difficulties mentioned above disappear if one assumes mass dependent amplitudes. Leaving the VMD identities of equations 4.9 and 4.10 unchanged, we make the following assumptions:

- A. The diffractive amplitude $f_{\rho\rho}$ is a function of the difference between the masses of the incoming and outgoing ρ -states, that is the amplitude $f_{\rho(m_{in}), \rho(m_{out})}$ which appears in the diagrams of fig. 8 is a function of $(m_{in}^2 - m_{out}^2)$.
- B. The amplitude $f(\rho^0 p \rightarrow \pi^+ n)$ which appears in the VMD description of π^+ photo-production reaction is a function of the mass of the virtual ρ^0 meson, as discussed elsewhere (46, 47).

Considering assumption (A), we find that the diffractive amplitude appearing in the diagram (b) of fig. 8 ($m_{in} \neq m_{out}$) may be different from the amplitude of the diagrams (a) and (c) ($m_{in} = m_{out}$). We express this difference by the factor λ which is defined by the generalization of equation 4.13

$$\frac{d\sigma}{dt}(\gamma P \rightarrow \rho^0 P)_{t=0} = \lambda^2 \frac{1}{16} \frac{g_{EM}^2}{4\pi} \left(\frac{\delta_R^2}{4\pi} \right)^{-1} \sigma_\rho^2 (1 + \beta^2)$$

For $\lambda = 1$ we have the usual VMD, for $\lambda \neq 1$ we have a mass dependent amplitude.

The value of λ can be determined by comparing the values of σ_ρ obtained from ρ^0 photo-production on hydrogen (see Table 4) and from photon total cross section measurements (see Table 5). We find λ to be essentially energy independent with a mean value of $\lambda = 0.9$. This means the change in mass from the incoming $m_\gamma = 0$

to the outgoing $m_\rho = 765$ MeV decreases the diffractive ($\rho N \rightarrow \rho N$) amplitude by a factor 0.9.

These assumptions affect the calculations of cross sections on nuclei in the following way:

(a) Photon-nucleus total cross sections:

The ratio of the contributions of the two-step process of fig.9b to the one-step process of fig. 9a decreases. Since the two-step amplitude interferes destructively with the dominating one-step amplitude, the total cross section increases. The result of the calculation is shown in fig. 13 (broken lines) and exhibits good agreement with the experimental data. We note that we have used the slightly larger values of σ_ρ given in Table 5.

(b) Incoherent π^+ photo-production:

Here, in addition, we must know the mass dependence of the production amplitude $f(\rho^0 p \rightarrow \pi^+ n)$ according to assumption (B). We use the value $\lambda_{\rho\pi} = \sqrt{0.5}$ for the ratio $f_{\rho\pi^+}(m_\rho = 765 \text{ MeV})/f_{\rho\pi^+}(m_\rho = 0)$. This value is obtained⁽⁴⁷⁾ by comparing experiments of π^+ photo-production with ρ production by pions on protons. The result of this is, as in the case of photon-nucleus total cross section calculations, that the two-step amplitude of fig. 10b decreases in ratio to the one-step amplitude of fig. 10a. Since the two-step amplitude interferes destructively with the dominating one-step amplitude, the effective number N_{eff}

increases appreciably. The detailed results are shown in fig. 14 (broken lines) and are in good agreement with the experimental data.

(c) Incoherent ρ^0 photo-production:

We note that the calculations of ρ^0 production on nuclei are not affected by the assumption of mass dependent amplitudes. However, there is a slight change in the value of σ_ρ which is now taken from Table 5.

We come to the conclusion that the VMD model, together with the eikonal methods used, provide a reasonable description of the photo-reactions on nuclei described above. However, if we allow for mass dependences of the diffractive ρ -nucleon amplitude $f(\rho N \rightarrow \rho N)$ and the production amplitude $f(\rho^0 p \rightarrow \pi^+ n)$, and if we determine these dependences from two-body reactions, we find that the calculations for photo-reactions on nuclei (photon-nucleus total cross sections and incoherent π^+ photo-production) show a better agreement with the experimental data. Up to now, the experimental uncertainties are too large to clearly decide whether the two-body amplitudes are mass dependent in the way discussed above.

4.3 Neutron-nucleus total cross sections

Recently there have been measurements of neutron total cross sections ⁽⁴⁸⁾ performed on Be, C, Al, Cu, and Pb with one per cent accuracy at average neutron momenta of 8, 11, 14 and 21 Gev/c. For all elements there is a smooth drop of about 3% between 8 and 21 Gev/c, very similar to that for the corresponding p-p and n-p total cross sections. Normalizing the cross sections to the n-p total cross section, no momentum dependence is observed. This is a little puzzling for the heavy nuclei, since one expects to be approaching the physical situation of a "black target" with a geometrical cross section, for a nucleus as heavy as lead. On the other hand, the energy dependence under consideration is rather weak and the blackness of the heavy nuclei is weakened if one includes the regenerative amplitude resulting from first diffractively producing nucleon isobars on one nucleon, and then having them regenerate a neutron (see fig. 15). To what extent the regeneration contributes is at this point to be answered through calculation. Pumplin and Ross ⁽⁴⁹⁾ have suggested that regenerative effects are quite strong, depleting total cross sections of heavy nuclei by some 20% at energies of the order of 20 to 30 Gev. The recent data do not bear this out, however, and we shall return to a discussion of this question below.

We have made calculations ⁽⁶⁾ of the elastic scattering of neutrons from nuclei using the coupled channel eikonal approach described in chapter 2, and taking into account regeneration of neutrons after production of the neutral charge state of the isospin 1/2 isobars N* (1400), N* (1520), N* (1688), N* (2190). In our calculation we

have represented the intermediate nucleon isobars in an average way by one N^* channel, with the average mass $m_{N^*} = 1520$ Mev. We can do this approximation because we find that the N^* contribution to the total cross section is only of the order of a few per cent. The production cross sections for the different isobars, taken from reference (50), are added together and give the value for the total N^* production cross section $\frac{d\sigma}{dt} (nN \rightarrow N^*N)_{t=0} = 7.5$ mb/GeV². The two-body parameters for neutron elastic scattering on protons and neutrons are listed in Table 6. The total cross section of the intermediate isobars on nucleons is taken to be $\sigma_{N^*} = 40$ mb. We have taken the phase $\beta = \text{Re } f(0)/\text{Im } f(0)$ to be equal for p-p and n-p scattering. We have also assumed the same phase for the diffractive production amplitudes. For the nuclear shape we have used the parameters from reference (25) listed in Table 1.

The results of our calculations are shown in fig. 16. The measurements and calculations agree very well. The effects of regeneration as included here are small as shown in fig. 16 for lead and carbon. We note now the uncertainty in nuclear radius, the small but non-negligible experimental errors in nucleon-nucleon total cross sections and β (which could change our results by ± 1 to 2%), and the neglect of nuclear correlations (+ 1 to 2% for short range correlations, 0 to 2% for deformation effects). Given all of this, it is not completely clear that the effect of N^* is manifest at present energies. However, for the heaviest nuclei, as seen in fig. 16 for lead, regeneration contributes in an energy dependent way to improve the energy dependence of the calculations when compared with experiment.

The authors of reference (49) include virtually the whole missing mass spectrum as contributions to the regenerative amplitude. The forward differential cross section from this spectrum is about half the forward elastic differential cross section. The fact that the regenerative amplitude is not nearly so strong as suggested in reference (49) could be the result of the following:

- (a) There are many diffractive amplitudes but with different phases and therefore much cancellation.
- (b) The non-resonant background included in the work of reference (49) is largely non-diffractive.
- (c) Non-resonant diffraction products spread too much before travelling a distance of the order of inter-nucleon spacing to generate a nucleon.

In connection with these possibilities, a careful study of incoherent scattering of nucleons from deuteron targets is of interest ⁽⁵¹⁾. Incoherent regeneration on the deuteron can still be expected to be rather strong if the weakness of coherent regeneration results from effects (a) or (b) above. It will be weak if effect (c) is responsible for the weakness of coherent regeneration, since the two nucleons in the deuteron are relatively far apart (≈ 2 fm). At the moment the data are not quite good enough to be definitive.

We note that a recent experiment ⁽⁵²⁾ indicates that point (b) is true. The experiment measures the N^* production cross section σ in the missing mass reaction $\pi p \rightarrow \pi N^*$. The authors para-

meterize the dependence of σ on the incident momentum p by the formula $\sigma \propto p^{-n}$, and find the value $n = 0.7 \pm 0.1$ for the background contribution, whereas for N^* production as well as for elastic scattering they find the value of n to be of the order of 0.2. This indicates that the background in the mass spectrum for this experiment is mostly non-diffractive. The authors point out the similarity between this experiment and proton-proton inelastic scattering.

5. THE EFFECT OF NUCLEAR CORRELATIONS

5.1 Introduction

In the calculations above we did not consider the effect that correlations between individual nucleons of the target nucleus can have on the reaction cross section. With the product density distribution of equation 2.1 we assume in fact that the nucleons inside the nucleus move independently of one another. On the other hand, we know that there are correlations between nucleons which are due to

- (a) the Pauli exclusion principle (Pauli correlations),
- (b) the interaction force between nucleons (dynamical correlations).

We distinguish

- (i) short range correlations that are characterized by a distance short compared to the nuclear radius. They can be induced by the Pauli exclusion principle and by a hard core repulsive interaction between the nucleons;
- (ii) long range correlations that involve distances of the order of the nucleus.

In what follows, we consider only the short range correlations in the nucleus.

For high energy reactions the contribution of these correlations to the cross section is generally small since it is

a contribution from a multi-step reaction, which takes place between the incoming particle and the nucleons that exhibit the correlation.

The effect of correlations to coherent amplitudes is most easily described^(1, 7, 53) by an effective increase of the two-body cross sections of the order of a few %. The effect of correlations on the incoherent reactions is characterized by a forward dip in the t -dependence of the differential cross section, the detailed form of which depends⁽⁷⁾ on the form of the correlations as well as on the damping of the reacting particles inside the nucleus.

There are several methods of determining the nuclear correlations. The most important ones are the following:

- (a) theoretical calculations which assume a certain form for the interaction force between the nucleons (see, for example, reference (53));
- (b) medium energy reactions (see, for example, reference (54));
- (c) high energy reaction experiments (see, for example, references (55) and (21)).

In order to have a consistent picture, these different descriptions should agree with one another. Unfortunately, the uncertainties are large: On the one hand, the form of the nuclear interaction is not very well known. On the other hand, in experiments, it is difficult to clearly separate the effect of correlations from other possible influences.

In the following we present a description ⁽⁷⁾ of high energy reactions of particles with nuclei, with special emphasis on the effect of correlations on cross sections. At this point it is important that we also consider the effect of the range of the two-body interaction, since it is not much smaller than the range of the correlations. Because of the smallness of the correlation corrections we now keep terms of the order of $1/A$ which are given by the Glauber multiple scattering model ⁽¹⁾, and which we have neglected in the optical model calculations above.

The following calculations are presented for the case of particle scattering of nuclei. We note that similar formulae hold for the case of diffractive and non-diffractive production reactions.

5.2 The definition of the correlation function

We restrict ourselves in the following to the discussion of two-body correlations, since the influence on high energy cross sections of correlations between three or more nucleons is expected to be very small indeed. We define the two-body correlation function $g(r_1, r_2)$ of the true nuclear ground state wave function \tilde{u}_T through the equation

$$\int d^3r_3 d^3r_4 \dots d^3r_A \left| \tilde{u}_T(r_1, r_2, r_3, \dots, r_A) \right|^2 = \rho(r_1) \rho(r_2) \left[1 + g(r_1, r_2) \right] \quad (5.1)$$

with the single particle density distribution

$$\rho(r_1) = \int d^3 r_2 d^3 r_3 \dots d^3 r_A \left| \tilde{u}_I(r_1, r_2, \dots, r_A) \right|^2 \quad (5.2)$$

From the normalisation of $\tilde{u}_I(r_1, \dots, r_A)$ and $\rho(r)$ follow the identities

$$\int d^3 r_1 d^3 r_2 \rho(r_1) \rho(r_2) g(r_1, r_2) = 0$$

and

$$\int d^3 r_1 \rho(r_1) g(r_1, r_2) = 0 \quad \text{for all } r_2,$$

which will be useful below. From now on we consider for the nuclear ground state the wave function u_I given by

$$\left| u_I(r_1, r_2, \dots, r_A) \right|^2 = \prod_{i=1}^A \rho(r_i) \left[1 + \sum_{i>j} g(r_i, r_j) \right] \quad (5.4)$$

which reproduces the same single particle density $\rho(r)$ and correlation function $g(r_1, r_2)$ as does the true wave function \tilde{u}_I .

The typical form of the correlation function $g(r_1, r_2)$ can be studied in simplified models, such as a simple Fermi gas model ⁽¹⁾ or in a model with a repulsive core interaction between nucleons ⁽⁵³⁾. In both cases the correlation function, $g(r_1, r_2) = g(r_1 - r_2)$, is translational invariant. One has

$g(0) = -1$, so that the wave function vanishes as the nucleons come together, and $g(r)$ approaches zero for distances r large compared to the typical range of the correlation, which is of the order of one fermi.

For the following calculations it is important to note that the value of the correlation range lies between the nuclear radius and the two-body interaction range, and is close to the latter.

5.3 Elastic Scattering

Within the Glauber multiple scattering theory ⁽¹⁾ the scattering amplitude of a particle on a nucleus near the forward direction is given by

$$F_{IF}(q) = \frac{iP}{2\pi} \int d^2b e^{iqb} \langle I | 1 - \prod_{i=1}^A \{ 1 - \Gamma(b-s_i) \} | F \rangle \quad (5.5)$$

where $|I\rangle$ and $|F\rangle$ designate the initial and final state of the nucleus, q is the momentum transfer and $\Gamma(b)$ is the two-body profile function defined in equation 2.4. For elastic scattering the nucleus remains in its ground state $|I\rangle$ and we have

$$F_{el}(q) = \frac{iP}{2\pi} \int d^2b e^{iqb} \langle I | 1 - \prod_{i=1}^A \{ 1 - \Gamma(b-s_i) \} | I \rangle \quad (5.6)$$

In order to evaluate the above formula we introduce for convenience the quantities

$$t(b) = \int d^3r \rho(r) \Gamma(b-s)$$

and

(5.7)

$$q(b) = \int d^3r_1 d^3r_2 \rho(r_1) \rho(r_2) g(r_1, r_2) \\ \times \Gamma(b-s_1) \Gamma(b-s_2)$$

where s represents the perpendicular component of the space vector $\vec{r} = (\vec{s}, z)$.

The quantity $t(b)$ is related to the nuclear profile function $T(b)$, defined in equation 2.17, in the following way: We define an effective density function

$$\rho_R(s, z) = \frac{ik}{2\pi f(0)} \int d^2s' \rho(s', z) \Gamma(s-s') \quad (5.8)$$

which is a folding of the density function $\rho(r)$ with the normalized two-body interaction $\frac{ik}{2\pi f(0)} \Gamma(s)$. In the limit of zero range interaction we have $\rho_R(r) = \rho(r)$. Thus the effective profile function

$$T_R(b) = A \int_{-\infty}^{\infty} dz \rho_R(b, z) \quad (5.9)$$

includes the effect of the two-body interaction range, and we can write

$$t(b) = \frac{2\pi f(0)}{ik} \frac{1}{A} T_R(b) = \frac{\sigma'}{2A} T_R(b) \quad (5.10)$$

with the quantity $\sigma' = \frac{4\pi f(0)}{ik} = \sigma(1 - i\beta)$ introduced in equation 4.2. We note that the value of $t(b)$ is usually of the order of $1/A$.

For the evaluation of the quantity $q(b)$ we make use of the following approximations:

- (A) We assume a gaussian form for the two-body interaction amplitude

$$f(q) = f(0) e^{-\frac{a}{2} q^2}$$

which yields with equation 2.4

$$T(b) = \frac{f(0)}{ika} e^{-\frac{b^2}{2a}}$$

- (B) We assume that the correlation function $g(r_1, r_2)$ is translational invariant, i.e.

$$g(r_1, r_2) = g(r_1 - r_2)$$

- (C) We assume the two-body interaction range to be short compared to the nuclear density structure.

- (D) We assume the correlation range to be short compared to the nuclear density structure.

In order to evaluate $q(b)$ given by equation 5.7 we introduce new coordinates (S, Z) and (s, z) by

$$s = \frac{1}{2} (s_1 + s_2) \quad ; \quad z = \frac{1}{2} (z_1 + z_2)$$

and

$$s = s_1 - s_2 \quad ; \quad z = z_1 - z_2$$

Using the approximations (A), (B), and (C) we find

$$q(b) = \frac{\nabla'^2}{16\pi a} \int dZ d^2s dz \\ \times \rho\left(b + \frac{s}{2}, Z + \frac{z}{2}\right) \rho\left(b - \frac{s}{2}, Z - \frac{z}{2}\right) g(s, z) e^{-\frac{s^2}{4a}}$$

Since for the d^2s and dz integration the variables $s/2$ and $z/2$ enter the two factors $\rho(b + s/2, Z + z/2)$ $\rho(b - s/2, Z - z/2)$ with opposite sign, the first order variation of the product cancels.

Therefore we can use (D) to good approximation, and write

$$q(b) = \frac{\nabla'^2}{16\pi a} \int dZ \rho^2(b, Z) \\ \times \int d^2s e^{-\frac{s^2}{4a}} \int dz g(s, z) \quad (5.11)$$

We define the correlation length ξ by

$$\xi = \frac{1}{16\pi a} \int d^2s e^{-\frac{s^2}{4a}} \int dz g(s, z) \quad (5.12)$$

and the quantity $Q(b)$ by

$$Q(b) = A^2 \int_{-\infty}^{\infty} dz \rho^2(b, z) \quad (5.13)$$

Then equation 5.11 can be written as

$$q(b) = \sigma'^2 \sum \frac{Q(b)}{A^2} \quad (5.14)$$

Now we go back to evaluate the equation 5.6 for the elastic amplitude $F_{el}(q)$. Using the density distribution of equation 5.4 and the identities of equations 5.3 we find that

$$\begin{aligned} \langle I | \prod_{i=1}^A \{1 - \Gamma(b - s_i)\} | I \rangle \\ = (1 - t(b))^A + \frac{1}{2} A(A-1) (1 - t(b))^{A-2} q(b) \\ \simeq \left(1 - t(b) + \frac{1}{2} A q(b)\right)^A \end{aligned}$$

We have used here the following approximation:

- (E) Compared to terms of the order of $At(b)$ we neglect terms of the order of $A^3 t(b)q(b)$, $A^4 q^2(b)$, and higher order terms involving $q(b)$. This is justified because a numerical evaluation shows that $At(b)$ is of the order of one and $Aq(b) \ll t(b)$.

With equations 5.10 and 5.14 we find that

$$\begin{aligned} \langle I | \prod_{i=1}^A \{1 - \Gamma(b - s_i)\} | I \rangle \\ = \left(1 - \frac{\sigma'}{2A} T_R(b) + \frac{\sigma'^2}{2A} \sum Q(b)\right)^A = \left(1 - \frac{\sigma'}{2A} T_C(b)\right)^A \end{aligned} \quad (5.15)$$

where

$$T_C(b) = T_R(b) - \sigma' \sum Q(b) \quad (5.16)$$

is the effective profile function of the nucleus that includes the effects of the two-body interaction range as well as the nuclear correlations. Using equation 5.15 and the expansion

$$\left(1 - \frac{x}{A}\right)^A = e^{-x} \left(1 - \frac{x^2}{2A}\right)$$

which neglects some terms of the order of $\frac{1}{A^2}$ and higher, we find for the elastic scattering amplitude given in equation 5.6 the expression

$$F_{el}(q) = f(0) \left\{ N^c(q; 0, \frac{\sigma'}{2}) + \frac{1}{A} N_2^c(q; \frac{\sigma'}{2}) \right\} \quad (5.17)$$

Here we have used the effective nucleon numbers N^c which are defined by

$$\begin{aligned} N^c(q; 0, \frac{\sigma'}{2}) &= \frac{2}{\sigma'} \int d^2b e^{iqb} \left\{ 1 - e^{-\frac{\sigma'}{2} T_c(b)} \right\} \\ N_m^c(q; \sigma) &= \frac{1}{m!} \frac{1}{\sigma} \int d^2b e^{iqb} \\ &\quad \times [\sigma T_c(b)]^m e^{-\sigma T_c(b)} \end{aligned} \quad (5.18)$$

We note that these effective numbers are generally complex numbers that take into account the two-body interaction range and the nuclear correlations.

We see that the effect of the interaction range and the nuclear correlations on the elastic scattering amplitude of equation 5.17 is shown by the replacement of the nuclear profile function $T(b)$ of equation 2.17 by the effective profile function $T_c(b)$ defined by

the equations 5.8, 5.9 and 5.16. For a repulsive correlation, such as the Pauli correlation, the correlation length ξ is negative and $T_c(b)$ is larger than $T(b)$. This means the probability for the incoming particle to have a reaction with some target nucleon is increased by the presence of nuclear correlations.

Another physical interpretation of this effect is to point out that the repulsive correlations decrease the probability that one nucleon is very close to another nucleon. Thus the screening of the nucleons by one another diminishes, and the probability for a reaction with the incident particle increases.

5.4 Summed cross section for elastic and inelastic scattering.

In high energy reaction experiments with nuclear targets it is often not possible to observe the final state of the nucleus. In this case one uses the closure relation

$$\sum_{\text{all states } |F\rangle} |F\rangle\langle F| = 1 \quad (5.19)$$

and assumes that the experiment determines the sum of reaction cross sections for all possible final nuclear states. For high energy reactions the closure approximation is good because the excitation energy of the final nuclear state is small compared to the energy of the incident particle.

For high energy scattering of particles on nuclei we have the summed cross section

$$\frac{d\sigma_{sc}}{d\Omega}(q) = \sum_{|F\rangle} |F_{IF}(q)|^2 = \sum_{|F\rangle} F_{IF}(q) F_{IF}^*(q) \quad (5.20)$$

where the summation runs over all possible final nuclear states $|F\rangle$.

We use equations 5.5 and 5.19 and get

$$\begin{aligned} \frac{d\sigma_{sc}}{d\Omega}(q) = & \frac{P^2}{4\pi^2} \int d^2b d^2b' e^{iq(b-b')} \left\{ 1 \right. \\ & - \langle I | \prod_{i=1}^A \{ 1 - \Gamma(b-s_i) \} | I \rangle \\ & - \langle I | \prod_{i=1}^A \{ 1 - \Gamma^*(b'-s_i) \} | I \rangle \\ & \left. + \langle I | \prod_{i=1}^A \{ (1 - \Gamma(b-s_i))(1 - \Gamma^*(b'-s_i)) \} | I \rangle \right\} \end{aligned} \quad (5.21)$$

The first terms in the bracket are the same as already evaluated for the elastic scattering amplitude (see equation 5.15). For the evaluation of the last term in the bracket we again use the density function of equation 5.4 and the identities 5.3. After some straightforward calculations where we use the approximation (E), described in the previous section, and the expansion

$$\begin{aligned} \left(1 + \frac{x}{A} + \frac{y}{A} \right)^A &= \left(1 + \frac{x}{A} \right)^A \left(1 + \frac{y}{A} \right)^A \\ &- \frac{xy}{A} \left(1 + \frac{x}{A} \right)^{A-1} \left(1 + \frac{y}{A} \right)^{A-1} \end{aligned} \quad (5.22)$$

which neglects some terms of the order of $\frac{1}{A^2}$ and higher, we can write the summed scattering cross section in the form

$$\begin{aligned} \frac{d\sigma_{sc}}{d\Omega}(q) = & \left| F_{el}(q) \right|^2 + \frac{k^2}{4\pi^2} \int d^2b \, d^2b' \times \\ & e^{iq(b-b')} \left(1 - t(b, b') + \frac{A}{2} q(b, b') \right)^{A-1} \times \\ & \left\{ -A t_c(b) t_c^*(b') (1 - t_c(b))^A (1 - t_c^*(b'))^A \right. \\ & + \left(t(b, b') - \frac{A}{2} q(b, b') \right) \times (1 - t_c(b) - t_c^*(b'))^A \\ & \left. + \frac{A^2}{2} (\tilde{q}(b, b') + \tilde{q}(b', b)) \times (1 - t_c(b) - t_c^*(b'))^A \right\} \end{aligned} \quad (5.23)$$

where the index c of $t_c(b)$ indicates that the correlation effect is included through

$$t_c(b) = t(b) - \frac{A}{2} q(b) \quad (5.24)$$

with $t(b)$ and $q(b)$ defined in the equations at 5.7.

The quantities $t(b, b')$, $q(b, b')$, and $\tilde{q}(b, b')$ are defined by

$$t(b, b') = \int d^3r \, \rho(r) \Gamma(b-s) \Gamma^*(b'-s) \quad (5.25)$$

$$q(b, b') = \int d^3 r_1 d^3 r_2 \rho(r_1) \rho(r_2) g(r_1, r_2) \times$$

$$\left\{ 2 \Gamma(b-s_1) \Gamma^*(b'-s_1) [\Gamma(b-s_2) + \Gamma^*(b'-s_2)] \right.$$

$$\left. - \Gamma(b-s_1) \Gamma^*(b'-s_1) \Gamma(b-s_2) \Gamma^*(b'-s_2) \right\} \quad (5.26)$$

$$\tilde{q}(b, b') = \int d^3 r_1 d^3 r_2 \rho(r_1) \rho(r_2) g(r_1, r_2) \times$$

$$\Gamma(b-s_1) \Gamma^*(b'-s_2) \quad (5.27)$$

Discussion of equation 5.23.

As expected, the summed scattering cross section $\frac{d\sigma_{sc}}{d\Omega}$ is the sum of the elastic scattering cross section $|F_{el}(q)|^2$ and contributions from reactions where the final nuclear state is excited. The first and higher order terms in the expansion of the factor $(1-t(b, b') + \frac{A}{2} q(b, b'))^{A-1}$ of equation 5.23 correspond to the contribution to the cross section by multiple-incoherent-step reactions (15, 19). From now on we restrict ourselves to the contribution from reactions with, at most, one incoherent step and therefore neglect this factor.

The contribution to the cross section from the first term in the bracket of equation 5.23 will be called the semi-coherent contribution and can be written in the form

$$\frac{d\sigma_{semi}}{d\Omega}(q) = -\frac{1}{A} |f(0)|^2 |N_1^c(q; \frac{\sigma'}{2})|^2 \quad (5.28)$$

with the effective number N_1^C defined in equation 5.18. The characteristics of the semi-coherent contribution is

- (i) its t -dependence which, like that of the elastic cross section, is determined by the shape of the nucleus, and
- (ii) the fact that it is negative and about a factor $\frac{1}{A}$ smaller than the elastic cross section.

The second term in the bracket of equation 5.23 gives rise to the incoherent cross section which is characterized by a t -dependence equal to that of the two-body differential cross section. We find that

$$\frac{d\sigma_{inc}}{d\Omega}(q) = |f(q)|^2 N_{eff}(\sigma, \xi) \quad (5.29)$$

with

$$N_{eff}(\sigma, \xi) = \int d^2b e^{-\sigma T_c(b)} \times (T(b) - 4\xi \sigma Q(b)) \quad (5.30)$$

We note that σ is the non-complex total cross section of the two-body interaction. In order to derive the term $-4\xi \sigma Q(b)$ in equation 5.30 we have used the short range approximation (C) and have assumed that

- (F) the two-body interaction range is short compared to the typical correlation distance.

The last term in the bracket of equation 5.23 gives rise to a contribution, which we call the correlation cross section, with a t -dependence typical of the correlation function. We find that

$$\frac{d\sigma_{\text{corr}}}{d\Omega}(q) = |f(q)|^2 G(q) \times \int d^2b Q(b) e^{-\sigma T_c(b)} \quad (5.31)$$

where

$$G(q) = \int d^3r e^{iqr} g(r) \quad (5.32)$$

is the three-dimensional Fourier transform of the correlation function $g(r)$. We obtain this result by using the identity (15)

$$\int d^2s \Gamma(b-s) \Gamma^*(b'-s) = \frac{1}{k^2} \int d^2q e^{-iq(b-b')} |f(q)|^2$$

together with the approximations (B) and (D) discussed in the previous section. We note that equation 5.31 holds for values of q large compared to $1/R$, R being the nuclear radius. For the region of smaller values of q , where elastic scattering is dominant, long range correlations, which we have neglected in our calculations, become important.

The summed scattering cross section then is given by

$$\frac{d\sigma_{\text{se}}}{d\Omega}(q) = |F_{\text{el}}(q)|^2 + \frac{d\sigma_{\text{semi}}}{d\Omega} + \frac{d\sigma_{\text{Inc}}}{d\Omega} + \frac{d\sigma_{\text{corr}}}{d\Omega} =$$

$$\frac{d\sigma_{sc}}{d\Omega}(q) = |f(0)|^2 \times \quad (5.33)$$

$$\left\{ |N^c(q; 0, \frac{\sigma'}{2})|^2 + \frac{2}{A} \operatorname{Re} \left\{ N^c(q; 0, \frac{\sigma'}{2}) N_2^{c*}(q; \frac{\sigma'}{2}) \right\} - \frac{1}{A} |N_1^c(q; \frac{\sigma'}{2})|^2 \right\}$$

$$+ |f(q)|^2 N_{\text{eff}}(\sigma, \xi) \left[1 + \eta(\sigma) G(q) \right]$$

Here we have used the equations 5.23, 5.17, 5.28, 5.29 and 5.31 and have dropped some terms quadratic in $\frac{1}{A}$ or in $g(r)$. The effective numbers N^c and N_{eff} are defined by the equations 5.18 and 5.30, and $G(q)$ is the Fourier transform of the correlation function $g(r)$. We have introduced the parameter

$$\eta(\sigma) = \frac{\int d^2b Q(b) e^{-\sigma T(b)}}{\int d^2b T(b) e^{-\sigma T(b)}} \quad (5.34)$$

whose value depends on the shape of the nucleus. For the Fermi gas model we have $\eta(\sigma) = \rho = \frac{A}{\text{Volume}}$. For more realistic density distributions, such as square well or Wood-Saxon densities, we find that $\eta(\sigma)$ is smaller and decreases with increasing two-body cross section σ . This σ -dependence is more pronounced for heavier nuclei. The smaller value of $\eta(\sigma)$ can be explained by the fact that a large portion of the cross section is due to reactions that take place at the surface of the nucleus where the nuclear density is smaller. Values of $\eta(\sigma)$ are listed in Table 7.

At this point it is important to note that, for the above calculations, we have used the assumption (B) that the correlation

function $g(r_1, r_2)$ is translational invariant, which implies that $g(r)$, with $r = r_1 - r_2$, is the same in the center and at the surface of the nucleus although the nuclear density is quite different. This assumption is difficult to justify, although it could be tested for Pauli correlations by means of calculations with anti-symmetrized wave functions (56).

5.5 Discussion

Nuclear correlations affect the cross sections for high energy reactions in the following two ways:

- (a) The strength of the coherent and semi-coherent scattering amplitude as well as the damping for any other reaction is affected by the introduction of the effective nuclear profile function $T_c(b)$ of equation 5.16, which includes the contribution from nuclear correlations. This contribution is proportional to the two-body total cross section σ and the nuclear correlation length ξ defined in equation 5.12.
- (b) There is a direct contribution to the summed cross section, namely the correlation cross section of equation 5.31. It produces a forward dip in the inelastic cross section, and is characterized by a t -dependence given by the Fourier transform of the correlation function $g(r)$.

The above calculations are done for the case of scattering, where the incident and outgoing high energy particles are the same. Similar results are obtained for the case of production reactions. For diffractive production reactions, such as $\pi \rightarrow A_1$ and $\gamma \rightarrow \rho^0$, as for scattering, the coherent forward peak of the differential cross section overshadows the forward dip due to the correlation cross section. However, for non-diffractive reactions, such as charge exchange reactions and charged pion photo-production, the coherent cross section is not present.

The experiment of π^+ photo-production of reference (44) shows a forward dip in the differential cross section. This dip reflects the repulsive correlation of nucleons inside the target nucleus due to some repulsive core interaction as well as to the Pauli exclusion principle. Thus, the π^+ photo-production data gives information about the correlation function $g(r)$ (21).

We have used different estimates (21, 53, 54) for $g(r)$ to evaluate the correlation length ξ , defined in equation 5.12. It is to be noted that the two-body interaction range diminishes the effect of the correlations. In particular, the value of ξ decreases roughly by a factor of 0.5 compared to the value for the zero range interaction if we use the value $a = 8 \text{ Gev}^{-2}$ for the slope of the two-body differential cross section. We find ξ to be of the order of -0.3 fm.

The above calculations for the effects of nuclear correlations on high energy cross sections are valid for scattering and production reactions as long as the effect of longitudinal momentum

transfer can be neglected. Longitudinal momentum transfer effects have been described by the multi-channel optical model in chapter 2. We now give a prescription for how the effect of nuclear correlations, apart from the correlation cross section of equation 5.31, can be taken into account in optical model calculations.

One way of doing this is to replace the nuclear density function $\rho(b, z)$ in equation 2.3 or 2.5 by the effective density

$$\rho_c(b, z) = \rho(b, z) \left[1 - \sigma' \int A \rho(b, z) \right] \quad (5.35)$$

in analogy with the replacement of $T_R(b)$ by $T_C(b)$ in the calculation of coherent amplitudes according to equation 5.16.

On the other hand, one can introduce effective two-body amplitudes. We neglect the small change of the t -dependence of the differential cross section introduced by the nuclear correlations through equation 5.35 and by the two-body interaction range through equation 2.3, which can be accounted for by a measurement of an effective nuclear shape (see section 3.1 and reference (25)). We approximate the elastic scattering amplitude $F_{el}(q)$ of equation 5.17 by $F_{el}(q) = f(o) N^c(q; 0, \frac{\sigma'}{2})$ and define the effective two-body amplitude $f_E(o)$ and effective cross section $\sigma'_E = \sigma' f_E(o)/f(o)$ such that

$$f(o) N^c(o; 0, \frac{\sigma'}{2}) = F_{el}(o) = f_E(o) N(o, \frac{\sigma'_E}{2}) \quad (5.36)$$

where $N(0, \frac{\sigma'_E}{2})$, defined by equation 2.16, is equal to $N^C(0; 0, \frac{\sigma'}{2})$ in the absence of correlations. The effective two-body scattering amplitude, defined in this way, can be used in the optical model calculations if nuclear correlations are to be taken into account.

Using the equations 5.36, 5.18 and 5.16 we find that the effective two-body total cross section σ_E is given to good approximation by the A-dependent expression

$$\sigma_E = \sigma \left[1 - \xi \eta\left(\frac{\sigma}{2}\right) \sigma \right] \quad (5.37)$$

with the quantities ξ and $\eta(\sigma)$ defined in equations 5.12 and 5.34. Some values for σ_E are listed in Table 8. The differences between σ_E and σ are of the order of 5 to 10 per cent for $\xi = -0.3$ fm, and they can perhaps be detected by careful experiments on nuclei using particles whose scattering amplitudes on nucleons are well determined.

6. CONCLUSIONS

The foregoing calculations show how high energy multi-step reactions on nuclei can be described with a multi-channel optical model formalism. We distinguish coherent and incoherent production steps. The damping of the high energy particles inside the nucleus is taken into account. Generally we find destructive interference between the one-step and two-step amplitudes. Accordingly, the cross section for incoherent production of diffractive channels at very high energy, such as A_1 production by pions and ρ^0 photo-production, is expected to be about half the value of what is predicted by simple one-step calculations. This is indicated by ρ^0 photo-production experiments⁽⁴²⁾. In the case of A_1 production by pions the non-diffractive background is strong and makes the experimental analysis of the incoherent cross section more difficult.

In the case of coherent production of higher mass resonances, such as A_3 meson production by pions, it is conceivable that two-step processes contribute considerably to the cross section, with lower mass resonances as intermediate states. Detailed calculations are presented for the π - A_1 - A_3 system for different assumptions about the two-body amplitudes.

Within the framework of vector dominance, detailed calculations of photo-reactions have been presented in order to compare the available experimental data with the theoretical results. Incoherent

ρ^0 photo-production, incoherent π^+ photo-production, and photon-nucleus total cross section experiments have been compared simultaneously in order to test the consistency of the theory. The parameters for the calculations are taken from experiment as well.

There have been suggestions for modifications of the vector dominance model; for example, further heavy vector mesons could be included in order to explain the data of photon reactions on nuclei. Within the experimental uncertainties, we have found reasonable agreement between the experiments and our calculations, which are based on the simple vector dominance model. If we modify the model so as to have amplitudes that depend on the masses of incoming and outgoing particles, we find that the agreement with experiment further improves.

We have discussed the importance of contributions to the neutron-nucleus total cross sections by intermediate nucleon isobars N^* via a two-step process. The comparison with experiment shows that this contribution is very small, from which it follows that only resonances contribute as intermediate states, but not the background of the mass distribution. This can be understood from a recent experiment⁽⁵²⁾ that indicates that this background is produced mostly non-diffractively, from which it follows that the background cannot contribute to the coherent two-step process.

The effect of nuclear correlations on high energy reactions has been examined. We have discussed how these effects can be incorporated into an optical model description by using an effective two-body amplitude. We find that the effect of correlations is

smaller than has been proposed by other authors (53). The reason for this is that we take the surface of the nucleus into account in a different way, and that we do not neglect the two-body interaction range which is not much smaller than the nuclear correlation distance.

REFERENCES

1. R.J. Glauber, in Lectures in Theoretical Physics, edited by W.E. Brittin et al. (Interscience, New York, 1959) vol.1, p.315.
2. M. Nauenberg, Phys. Rev. Lett. 22, 556 (1969).
S.J. Brodsky and J. Pumplin, Phys. Rev. 182, 1794 (1969).
B. Margolis and C.L. Tang, Nucl. Phys. B10, 329 (1969).
3. G. v. Bochmann and B. Margolis, Nucl. Phys. B14, (1969) 609.
4. G. v. Bochmann and B. Margolis, Phys. Rev. Lett. 23, 935, (1969).
5. G. v. Bochmann, B. Margolis and C.L. Tang, Phys. Rev. Lett. 24, (1970) 483.
6. G. v. Bochmann, O. Kofoed-Hansen and B. Margolis, Phys.Lett. 33B (1970) 222.
7. G. v. Bochmann, B. Margolis and C.L. Tang, Phys. Lett. 30B, (1969) 254.
8. D. Morrison, Phys. Review 165 (1968) 1699.
9. R.J. Glauber, in Proceedings of the Third International Conference on High Energy Physics and Nuclear Structure, Columbia 1969 (Plenum Press, N.Y.).
10. D.W.G.S. Leith, Lectures presented to Scottish Universities Summer School in Physics, July-August 1970.

11. J.J. Veillet, in Proceedings of the Topical Conference on High Energy Collisions of Hadrons, CERN 1968.
12. C. Bemporad et al., Coherent Production of Pion Systems on Different Nuclei, paper submitted to XVth Intern. Conf. on High Energy Physics, Kiev (1970).
13. H. Foeth et al., Physics Letters 31B (1970) 544.
14. S.D. Drell and J.S. Trefil, Phys. Rev. Letters 16 (1966) 552.
15. K.S. Kölbig and B. Margolis, Nuclear Phys. B6 (1968) 85.
16. A.S. Goldhaber, C.J. Joachain, H.J. Lubatti and J.J. Veillet, Phys. Rev. Letters 22 (1969) 802.
17. K. Gottfried and D.R. Yennie, Phys. Rev. 182, 1595 (1969).
18. K. Gottfried, Quantum Mechanics (W.A. Benjamin, Inc. 1966).
19. R.J. Glauber and G. Matthiae, Report ISS 67/16, Istituto Superiore di Sanita, Laboratori di Fisica, Roma (1967).
20. G. McClellan et al., Phys. Rev. Letters 22 (1969) 374.
21. C.L. Tang, PhD Thesis at McGill University, Montreal, 1970.
22. H. Pilkuhn, in Proceedings of the 3rd Intern. Conf. on High Energy Physics and Nuclear Structure, Columbia 1969 (Plenum Press 1970).
23. L.R.B. Elton, Nuclear Sizes (Oxford University Press, 1961).
24. R. Hofstadter, Revs. Mod. Phys. 103 (1956) 1454.
25. H. Alvensleben et al., Phys. Rev. Letters 24 (1970) 786.

26. H. Alvensleben et al., Phys. Rev. Letters 24 (1970) 792, and Nuclear Physics B18 (1970) 333.
27. F. Bulos et al., Phys. Rev. Letters 22 (1969) 490.
G. McClellan et al., Phys. Rev. Letters 22 (1969) 377.
28. S.C.C. Ting, Proceedings of the 14th International Conference on High Energy Physics, Vienna, 1968.
29. A.N. Cnops et al., Phys. Rev. Letters 25 (1970) 1132.
30. M. Aderholz et al., Nucl. Phys. B8 (1968) 45.
J. Bartsch et al., Nucl. Phys. B7 (1968) 345.
31. G. Bellini, E. Fiorini, A.J. Herz, P. Negri and S. Ratti, Nuovo Cimento 29 (1963) 896.
F.R. Huson and W.B. Fretter, Nuovo Cimento 33 (1964) 1.
J.F. Allard et al., Nuovo Cimento 46A (1966) 737.
32. S. Frautschi and B. Margolis, Nuovo Cimento 56A (1968) 1155;
57A (1968) 427.
M. Jacob and S. Pokorski, Nuovo Cimento 61 (1969) 233.
33. H. Joos, Physics Letters 24B (1967) 103.
H.J. Lipkin and F. Scheck, Phys. Rev. Letters 16 (1966) 71.
34. H. Joos, in Proceedings of the Heidelberg Intern. Conf. on Elementary Particles (North Holland 1968) p. 359.
J.J. Sakurai, Summer Institute for Theoretical Physics, Boulder, Colorado, 1968.
35. K.J. Foley et al., Phys. Rev. Letters 19 (1967) 193.
H.I. Saxer, University of Michigan Technical Report 03106-19-T (1964).

36. H. Alvensleben et al., Nuclear Physics B25 (1971) 342.
37. H. Alvensleben et al., Phys. Rev. Letters 23 (1969) 1058.
38. D.O. Caldwell et al., Phys. Rev. Letters 23 (1969) 1256.

see also: D.O. Caldwell et al., Phys. Rev. Letters 25
(1970) 609.
39. H. Meyer et al., Total cross section for Photo-production of
hadrons on protons between 1.5 and 6.3 GeV, quoted in
reference 10, to be published.
40. R. Marshall, DESY preprint 70/32, July 1970.
41. Y. Sumi, Progr. of Theor. Physics, Supplements 41 and 42 (1967).
42. G. McClellan et al., Phys. Rev. Letters 23 (1969) 554.
43. J.G. Asbury et al., Phys. Rev. Letters 19 (1967) 865.
44. A.M. Boyarski et al., Phys. Rev. Letters 23 (1969) 1343.
45. H. Meyer et al., private communication and quoted by A. Silverman
in Proceedings of the 4th Intern. Symp. on Electron and
Photon Interactions at High Energies, Liverpool, 1969.
46. D. Schildknecht, in Proceedings of the Intern. Seminar "Vector
Mesons and Electromagnetic Interactions", Dubna, USSR,
September 1969.

W. Schmidt and D.R. Yennie, Phys. Rev. Letters 23 (1969) 623.
47. R. Diebold and J.A. Poirier, Phys. Rev. Letters 22 (1969) 906.

48. J. Engler et al., Phys. Letters 32B (1970) 716.
49. J. Pumplin and M. Ross, Phys. Rev. Letters 21 (1968) 1778.
50. E.W. Anderson et al., Phys. Rev. Letters 19 (1966) 855.
51. J.V. Allaby et al., Phys. Letters 30B (1969) 549.
52. E.W. Anderson et al., Experimental Study of $\pi^- + p \rightarrow \pi^- + N^*$ at 8 and 16 GeV, Brookhaven National Laboratory preprint 6/25/70.
53. E.J. Moniz and G.D. Nixon, Phys. Letters 30B (1969) 393.
54. F.C. Khanna, Phys. Rev. Letters 20 (1968) 871.
55. O. Kofoed-Hansen and C. Wilkin, CERN preprint TH 1194 (1970) to be published in the de Shalit Memorial Volume.
56. O. Kofoed-Hansen, in Proceedings of the Summer Institute on Diffractive Processes, McGill University 1969, to be published.
57. C. Wilkin, in Proceedings of the Summer Institute in Nuclear and Particle Physics, McGill University 1967 (W.A. Benjamin, Inc.).
58. K.J. Foley et al., Phys. Rev. Letters 19 (1967) 857.
59. J. Engler et al., Phys. Letters 31B (1970) 669.
60. L. Di Lella, in Proc. of the Heidelberg Intern. Conf. on Elementary Particles. (North Holland 1968) p. 164.
61. J. Engler et al., Phys. Letters 28B (1968) 64.

62. E.F. Parker et al., Phys. Letters 31B (1970) 250.

TABLE 1

The nuclear radius parameter R for a Wood-Saxon density distribution is given for different nuclei. The values from ref.(25) are obtained from a fit to the experimental data of coherent ρ^0 photo-production. The nuclear surface parameter is fixed to the value $c = 0.545$ fm.

Element	Atomic weight A	R in fm
Be	9.0	2.35 ± 0.26
C	12.0	2.50 ± 0.23
Al	27.0	3.37 ± 0.16
Cu	63.5	4.55 ± 0.11
Ag	107.9	5.35 ± 0.09
Pb	207.2	6.82 ± 0.20

TABLE 2

Integrated coherent meson production cross section normalized to the forward differential production cross section on protons: $\sigma^{(c)} / \frac{d\sigma^o}{dt}$ (o) in GeV^2 for the parameters as listed for fig. 6 .

	A=19	A=208	A = 64						
	16GeV	16GeV	∞ energy	16GeV	10GeV	5GeV	3GeV		
A_1 prod.	$\sigma_{A_1} = \sigma_{\pi}$	$\left\{ \begin{array}{l} R = 1.4 \\ R = 0.7 \\ R = -0.7 \end{array} \right.$	0.94	3.4	2.5	2.2			
			0.96	3.4	2.5	2.2	1.7	0.40	0.021
			1.03	3.7	3.0	2.4			
	$\sigma_{A_1} = \frac{1}{2}\sigma_{\pi}$	R = 1.4	1.32	7.4	4.4	3.8			
A_3 prod.	$\sigma_{A_1} = \sigma_{\pi}$	$\left\{ \begin{array}{l} R = 1.4 \\ R = 0.7 \\ R = -0.7 \end{array} \right.$	0.19	0.68	0.49	0.22			
			0.36	0.40	1.23	0.42	0.095	0.005	0.00002
			0.96	2.80	5.0	2.13			
	$\sigma_{A_1} = \frac{1}{2}\sigma_{\pi}$	R = 1.4	0.33	0.55	1.01	0.35			

The values of $\sigma^{(c)}$ are obtained by integrating $(d\sigma^{(c)}/dt)(t)$ from $t = t_{\min}$ up to $t \approx -0.1 \text{ GeV}^2$ for $A = 19$ and up to $t \approx -0.05 \text{ GeV}^2$ for $A = 64$ and $A = 208$.

TABLE 3

Effective number N_{eff} for incoherent meson production
for the parameters as listed for fig. 6.

	A=19	A=208	A = 64					
	16GeV	16GeV	∞ energy	16GeV	10GeV	5GeV	3GeV	
'one-step'	7.0	16.0	11.5	11.5	11.5	11.5	11.5	
Multi-step: pion incoh. scat.	6.8	15.6	11.0	11.1	11.2	11.5	11.5	
A_1 prod.	$\sigma_{A_1} = \sigma_{\pi} \left\{ \begin{array}{l} R = 1.4 \\ R = 0.7 \\ R = -0.7 \end{array} \right.$	3.3	8.8	4.0	5.1		11.5	
		3.3	8.9	4.2	5.2	6.6	10.2	11.5
		3.6	9.6	4.4	5.6			11.5
	$\sigma_{A_1} = \frac{1}{2}\sigma_{\pi} \quad R = 1.4$	4.6	12.4	5.5	7.2			16.7
A_1 prod.	$\sigma_{A_1} = \sigma_{\pi} \left\{ \begin{array}{l} R = 1.4 \\ R = 0.7 \\ R = -0.7 \end{array} \right.$	2.8	8.2	4.8	5.2		11.8	
		3.4	8.5	3.9	5.8	7.6	10.8	11.8
		7.0	23.	6.3	13.6			11.9
	$\sigma_{A_1} = \frac{1}{2}\sigma_{\pi} \quad R = 1.4$	3.4	9.4	4.7	6.1			11.9

TABLE 4

Photo-nucleon cross sections

The parameters for the two-body amplitudes of photon-reactions are listed as functions of the incident photon energy (see section 4.2.2.)

incident energy E_γ in GeV	3	5	8	16
$\frac{d\sigma}{dt} (\gamma p \rightarrow \rho^0 p)_{t=0}$ in $\mu\text{b}/\text{GeV}^2$ (fit to experimental data)	152	124	113	106
$\beta = \frac{\text{Re } f}{\text{Im } f}$	-.26	-.22	-.185	-.135
σ_p in mb determined from the values of $\frac{d\sigma}{dt} (\gamma p \rightarrow \rho^0 p)$ with VMD and $\frac{Y^2}{4\pi} = 0.5$	27.6	25.2	24.2	23.6
σ_{π^+} in mb			25.	24.

TABLE 5

The two-body total cross section σ_ρ
determined from the photon-nucleon total
cross section σ_γ (see section 4.2.6).

incident energy E_γ in GeV	5	8	16
σ_γ in μb (fit to experimental data)	124	117	111
σ_ρ in mb	28.5	26.8	25.5

TABLE 6

Neutron-nucleon cross sections

The parameters for the elastic two-body amplitudes are listed as functions of the incident neutron momentum.

Nucleon lab. momentum (GeV/c)	σ_{pp} (mb)	σ_{np} (mb)	$\beta = \frac{\text{Re } f(o)}{\text{Im } f(o)}$
5	41.0	40.5	-0.35
8	40.3	39.7	-0.33
14	39.4	38.7	-0.27
21	39.0	38.5	-0.20

σ_{pp} and β from ref. (58)

σ_{np} from refs. (59) and (60).

TABLE 7

The quantity $10 \eta(\sigma)$ in fm^{-3} for a Wood-Saxon nuclear density with $R = 1.14 A^{1/3}$ fm and $c = 0.545$ fm, as obtained from equation 5.34.

σ in mb	A =				
	208	108	64	27	20
5	1.07	.98	.89	.72	.65
7.5	1.02	.94	.86	.70	.64
10	.96	.89	.82	.68	.62
12.5	.90	.85	.79	.65	.60
15	.84	.80	.75	.63	.58
20	.71	.71	.68	.59	.55
25	.60	.61	.60	.54	.51
30	.51	.53	.54	.50	.47
35	.43	.46	.47	.46	.44
40	.37	.40	.42	.42	.41
50	.29	.31	.34	.35	.35

TABLE 8

The effective two-body total cross section σ_E as a function of σ for $\xi = -0.3$ fm and different values of A (See equation 5.37).

σ in mb	A =		
	208	64	27
10	10.3	10.3	10.2
20	21.2	21.0	20.8
30	33.3	32.0	31.7
40	43.4	43.2	42.8
50	54.5	54.5	54.1

FIGURE CAPTIONS

- Figure 1 One-step and multi-step contributions to the coherent production amplitude $F_{\alpha_1\alpha_2}$ on a nucleus.
- Figure 2 One-step and two-step processes for incoherent ρ^0 photo-production.
- Figure 3 One-step and two-step processes for incoherent production reactions.
- Figure 4 Processes with two incoherent steps that contribute to the π^+ photo-production cross section.
- Figure 5 The effective numbers $N_1(\sigma/2)$ and $N_2(\sigma/2)$ as functions of A for the nuclear parameters listed for figure 6.
- Figure 6 Differential cross section for A_1 meson production by incident pions on ^{64}Cu normalized to the cross section on protons: (a) $\sigma_{A_1} = \sigma_{\pi}$; $X = 0.7$
 (b) $\sigma_{A_1} = \frac{1}{2} \sigma_{\pi}$; $X = 1.4$

The parameters for the calculation are the following:

$$\sigma_{\pi} = \sigma_{A_3} = 26 \text{ mb}$$

$$\beta = 0 \quad \text{for all amplitudes}$$

$$\frac{d\sigma}{dt} (\pi p \rightarrow A_1 p)_{t=0} = 2.5 \text{ mb/GeV}^2$$

$$\frac{d\sigma}{dt} (\pi p \rightarrow A_3 p)_{t=0} = 0.3 \text{ mb/GeV}^2$$

The nuclear density is taken to be a Wood-Saxon distribution with $R = 1.14 A^{1/3}$ fm and $C = 0.545$ fm. For the calculation of the incoherent cross section an average value $a = 7.5 \text{ Gev}^{-2}$ is assumed for the slopes of all differential cross sections on protons.

Figure 7 Differential cross section for A_3 meson production by incident pions on ^{64}Cu normalized to the cross section on protons for the parameters listed for figure 6 and $\sigma_{A_1} = 26 \text{ mb}$

- (a) $X = 1.4$
- (b) $X = 0.7$
- (c) $X = -0.7$

Figure 8 Vector meson dominance diagrams for the diffractive two-body amplitudes of a photon γ , and a vector meson V on a nucleon N :

- (a) vector meson elastic scattering
- (b) vector meson photo-production
- (c) photon elastic scattering

Figure 9 Diagrams for photon forward elastic scattering on nuclei:

- (a) one-step elastic scattering of the photon
on a nucleon
- (b) two-step process with vector meson production
and photon regeneration

Figure 10 Diagrams for incoherent photo-production of the channel α on nuclei:

(a) one-step process

(b) two-step process with intermediate vector meson V .

Figure 11 Incoherent ρ^0 photo-production:

Experimental and theoretical values of N_{eff} are given for several energies as a function of A . The calculations are done for a Wood-Saxon nuclear density distribution with the parameters $R = 1.12 A^{1/3}$ fm and $C = 0.545$ fm. The effect of a change in the nuclear radius from $R = 1.12 A^{1/3}$ fm to $R = 1.18 A^{1/3}$ fm is shown for $A = 208$ at $E_\gamma = 5$ Gev.

Figure 12 Incoherent π^+ photo-production:

The A dependence of N_{eff} for four different momentum transfers. The normalization of the theoretical curves is fitted to the experimental data, for each value of momentum transfer. The nuclear parameters are listed for figure 11. The experimental errors are statistical only.

Figure 13 Photon-nucleus total cross sections:

Data from reference (38) is compared to the calculations of section 4.2.5. The nuclear parameters are listed for figure 11. The effect of a change in the nuclear radius from $R = 1.12 A^{1/3}$ fm to $R = 1.18 A^{1/3}$ fm is shown for $A = 208$ at $E_\gamma = 8$ Gev.

Full lines: two-body amplitudes from section 4.2.2.
 broken lines: mass dependent two-body amplitudes (see
 section 4.2.6).

Figure 14 Incoherent π^+ photo-production:

The values of N_{eff} are given for different nuclei
 normalized to the value for carbon.

The experimental data and the full line calculations are
 the same as in figure 12 (two-body amplitudes from
 section 4.2.2.)

The broken lines are calculations with mass dependent
 amplitudes (see section 4.2.6):

(a) incident photon energy 8 Gev

(b) incident photon energy 16 Gev.

Figure 15 Neutron-nucleus elastic scattering:

Diagram for the regenerative two-step amplitude.

Figure 16 Calculated and experimental values of neutron-nucleus
 total cross section. The effect of omitting the N^*
 contribution is shown for C and Pb.

solid lines: calculations using the nuclear parameters ⁽²⁵⁾
 listed in Table 1

broken lines: calculations using values for the nuclear
 radii which are at the upper and lower bound of
 of the experimental uncertainty.

Figure 17 (taken from reference 12)

Dependence of the production cross section $\pi^- + A \rightarrow \pi^+ \pi^- \pi^- + A$ for nuclei ranging from Be to Pb at 15.1 GeV/c. The cross sections refer to three-pion masses in the interval from 1 to 1.2 GeV. The incoherent events have been subtracted by fitting an exponential t' distribution to the (incoherent) tail of the angular distribution, the fraction of incoherent events in the integrated t' distribution varies from 35% in Be to 22% in Pb.

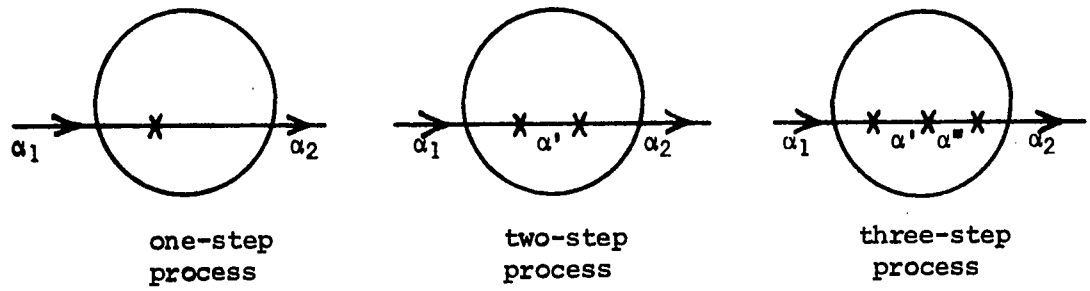


Fig. 1

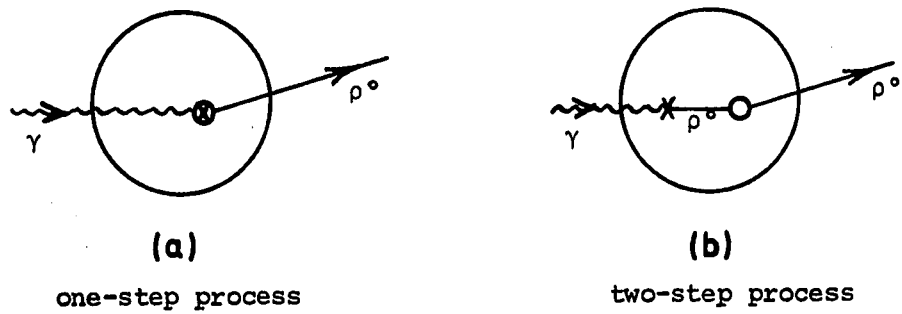


Fig. 2

Explanation of symbols:

- X— coherent production process: transition between channels.
- ⊗— incoherent production.
- incoherent scattering.

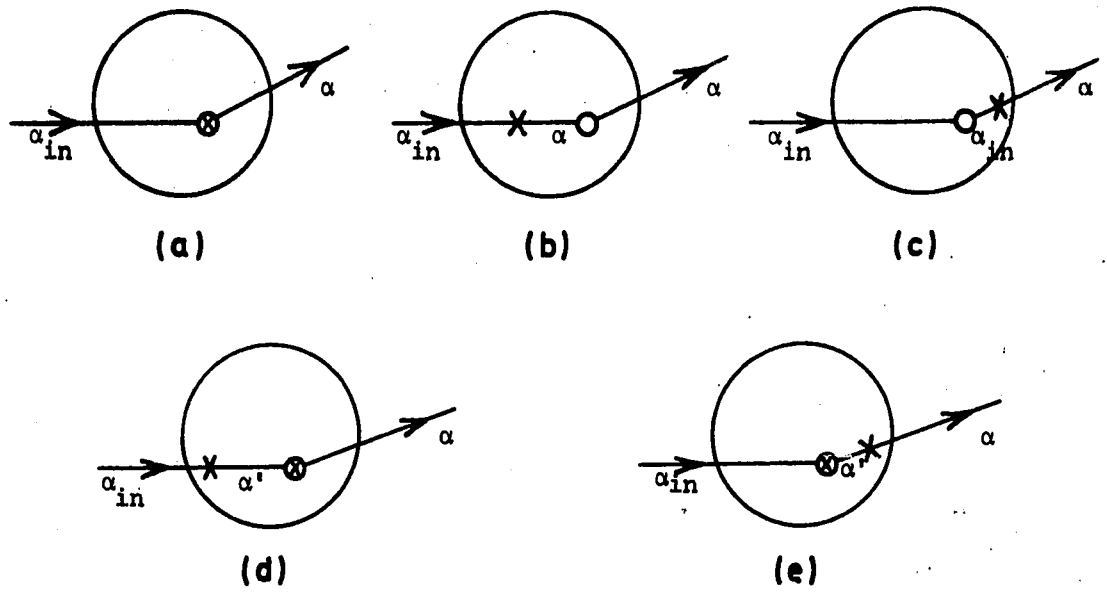


Fig. 3

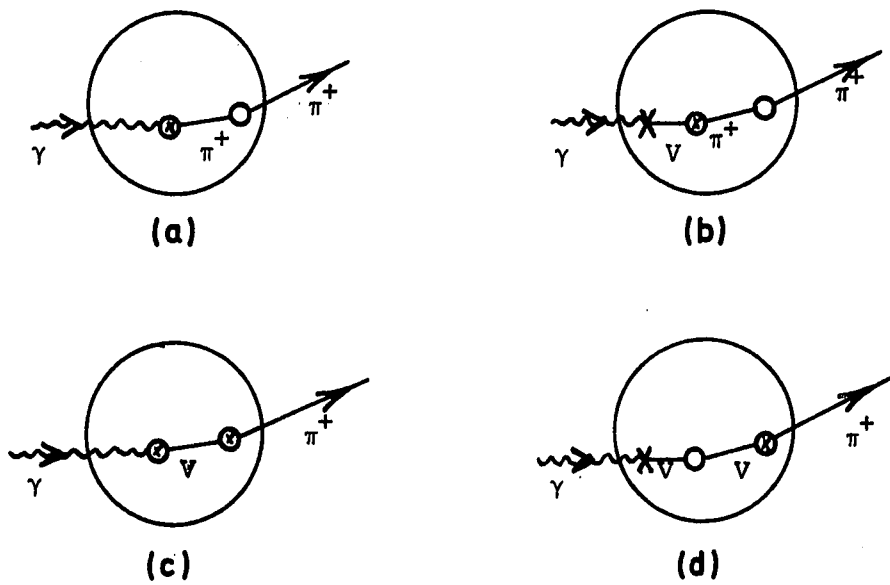


Fig. 4

Explanation of symbols:

- coherent production process: transition between channels.
- incoherent production.
- incoherent scattering.

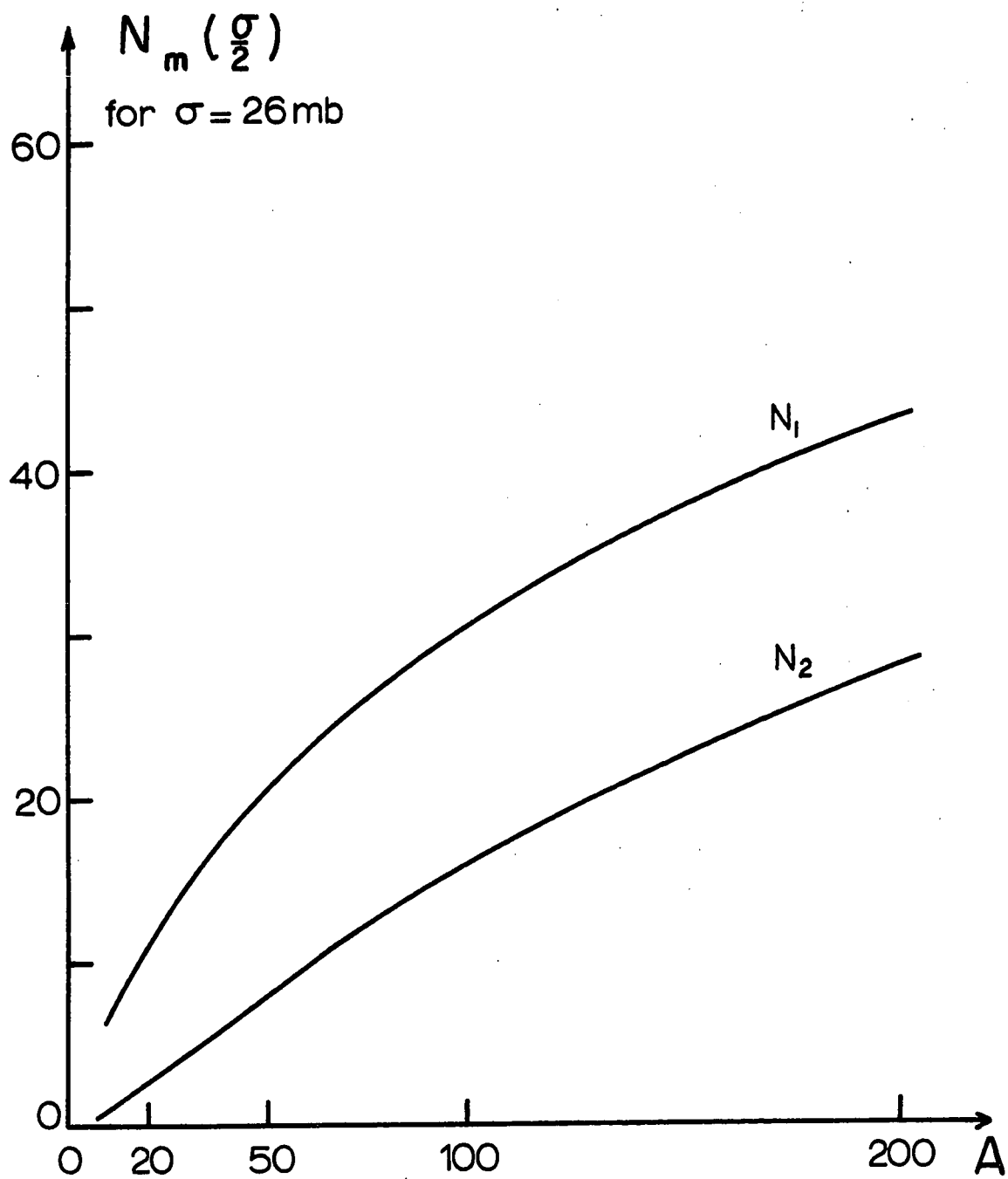


Fig. 5

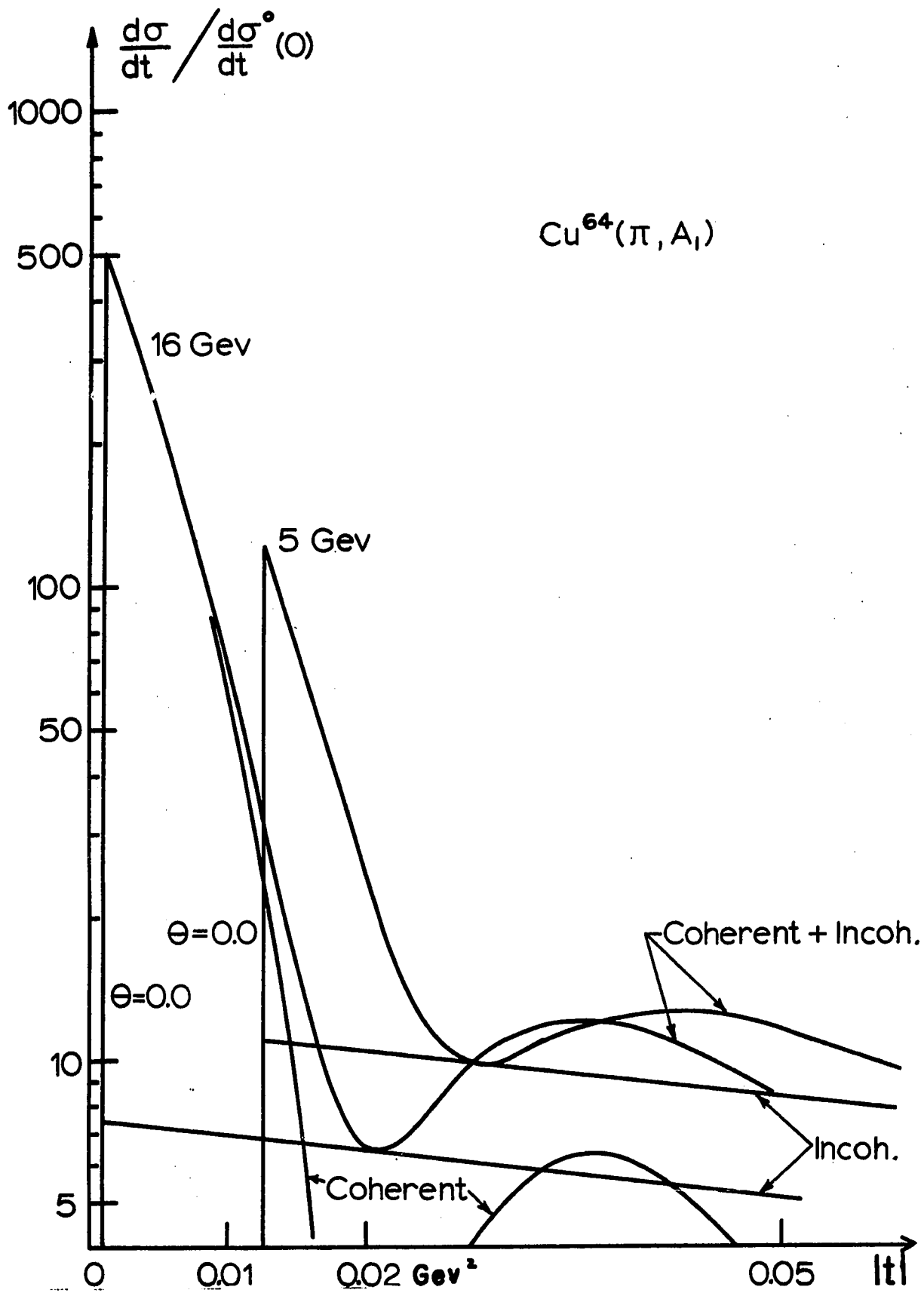


Fig. 6a

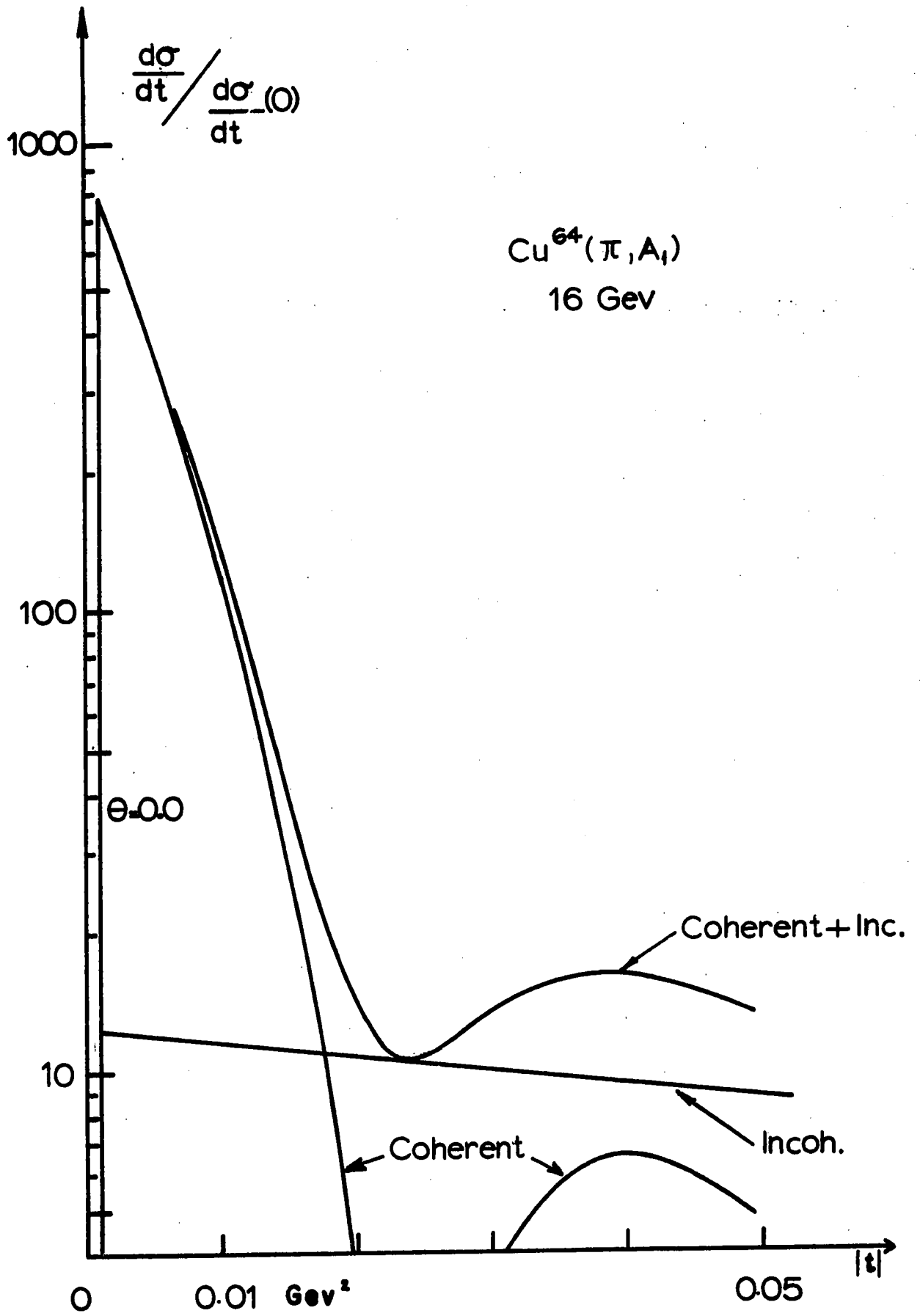


Fig. 6b

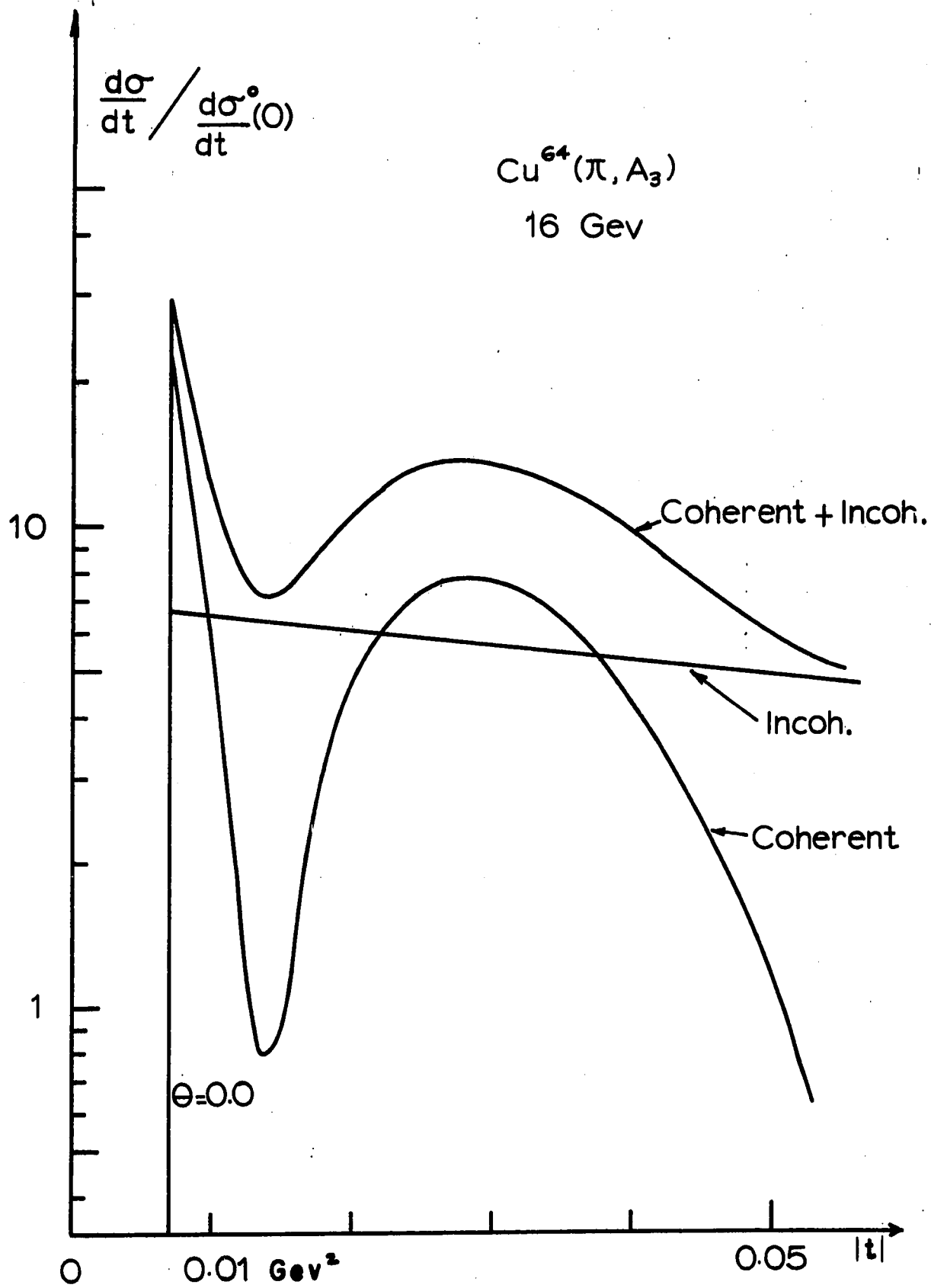


Fig. 7a

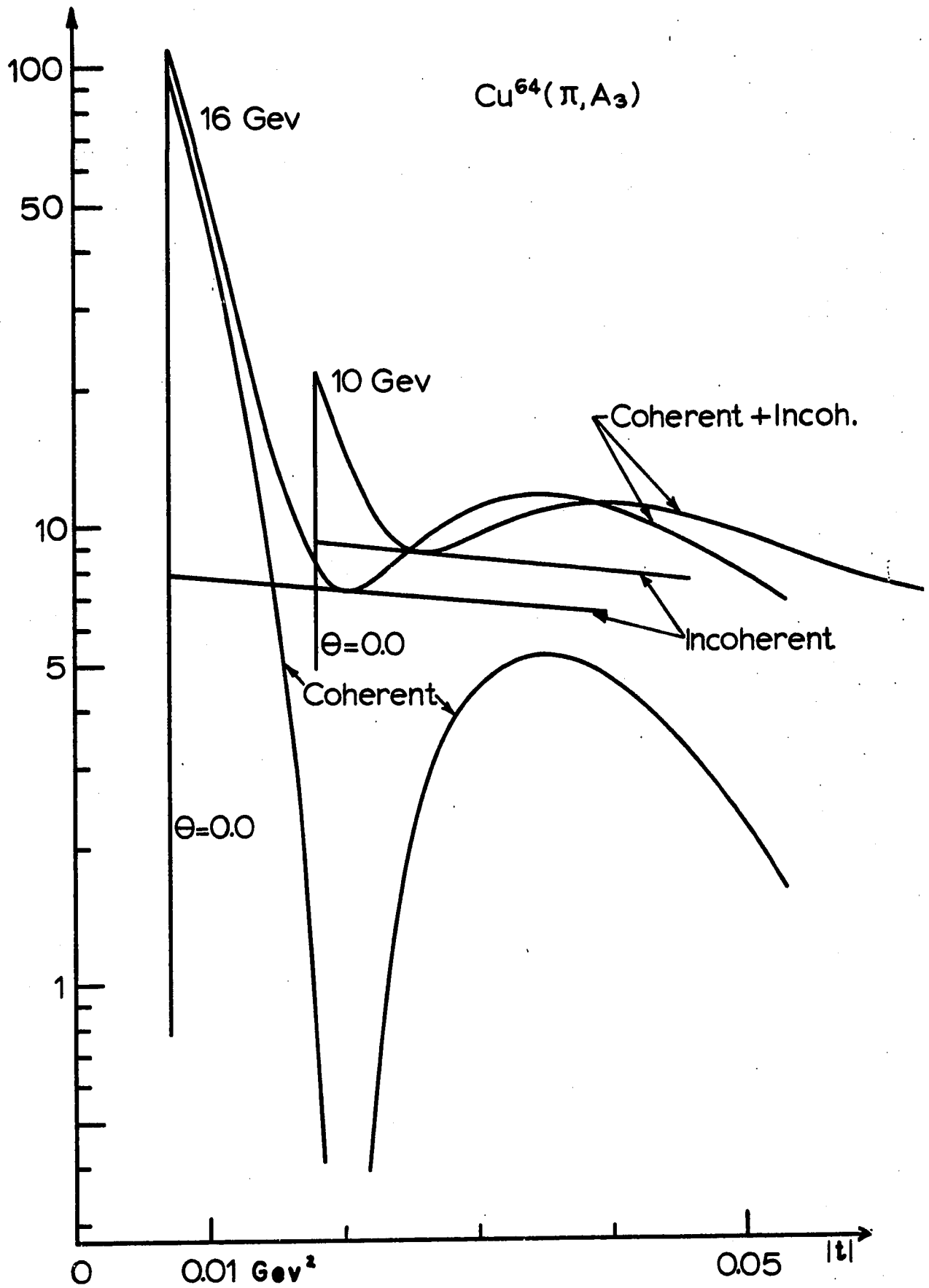


Fig. 7b

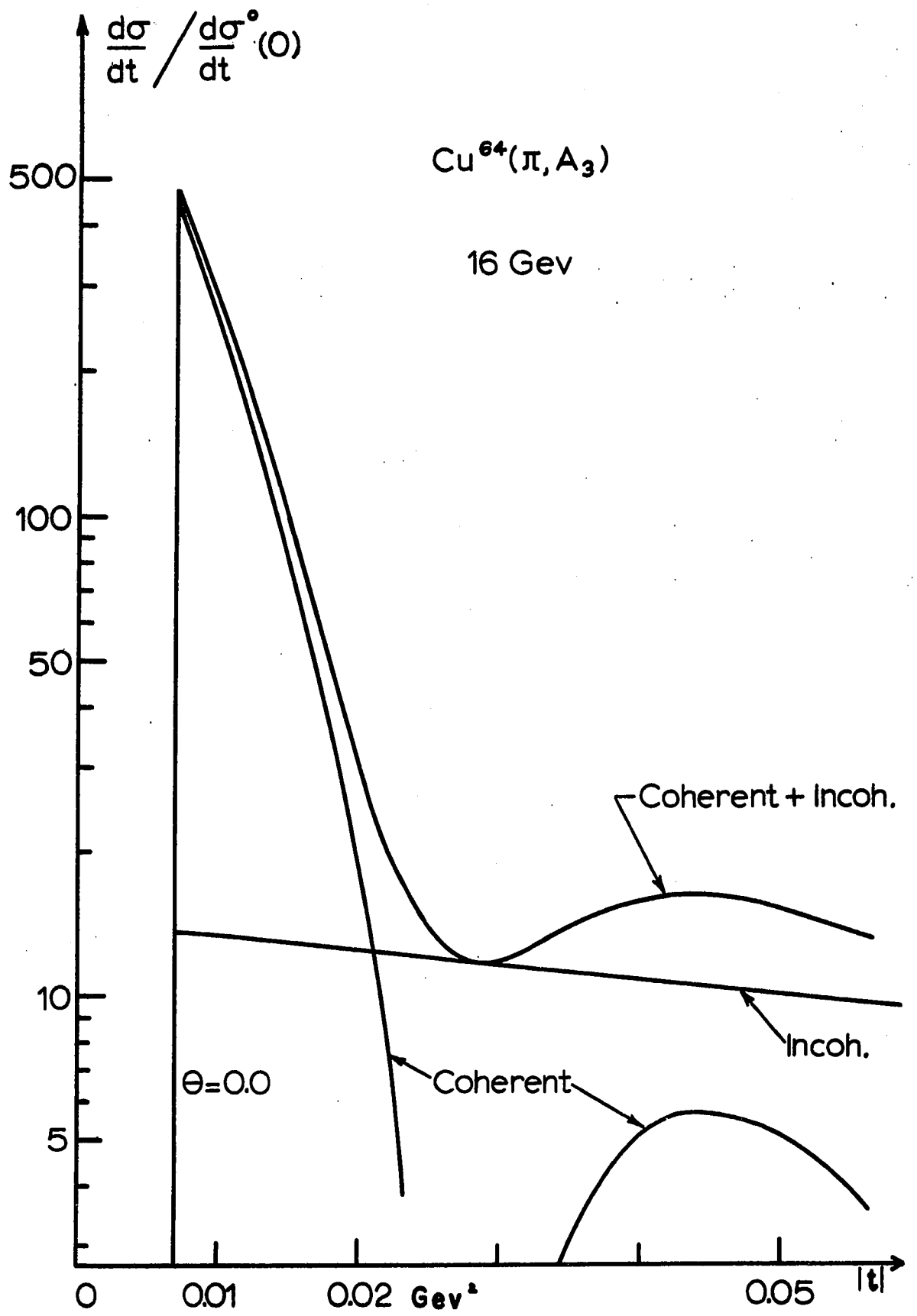


Fig.7c

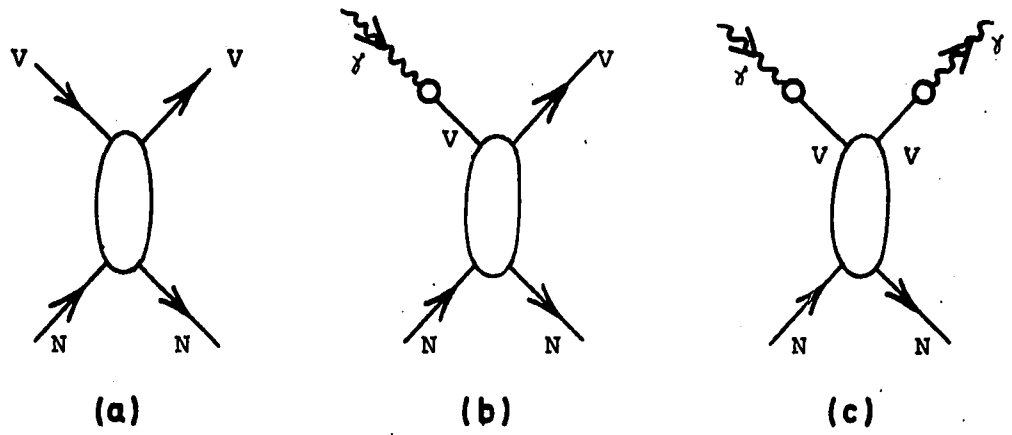


Fig. 8

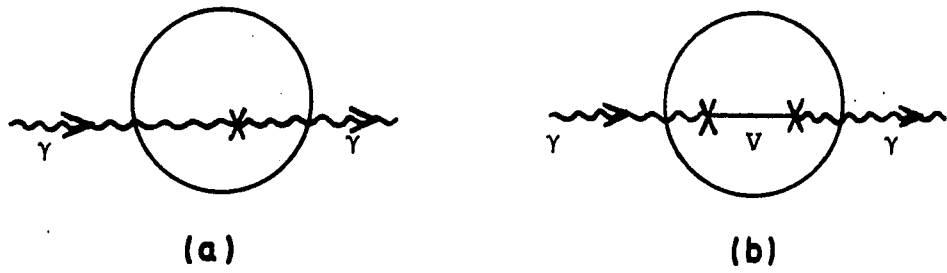


Fig. 9

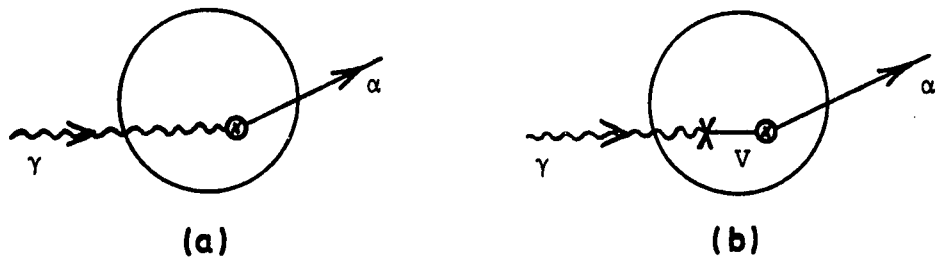


Fig. 10

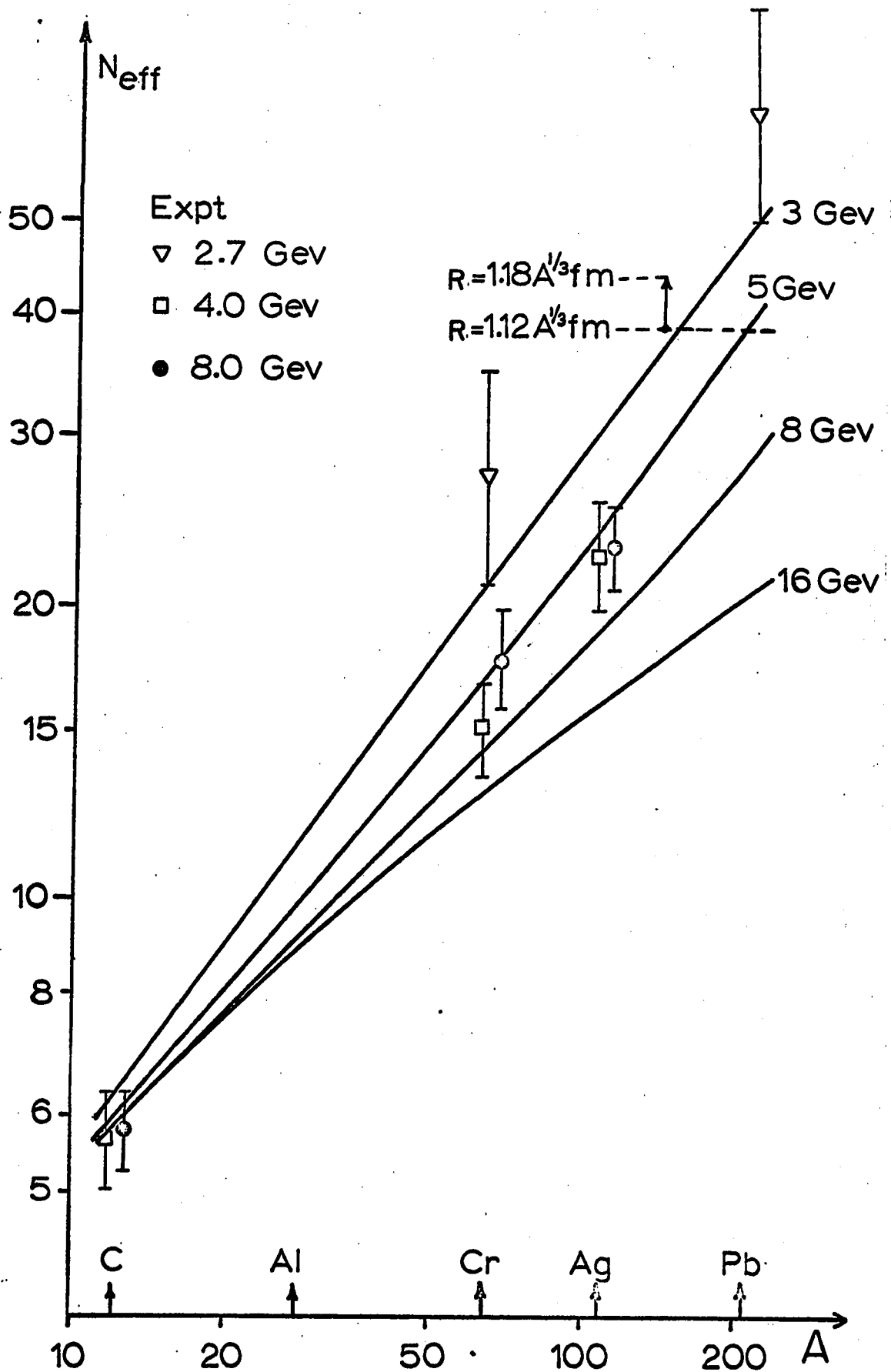


Fig. 11

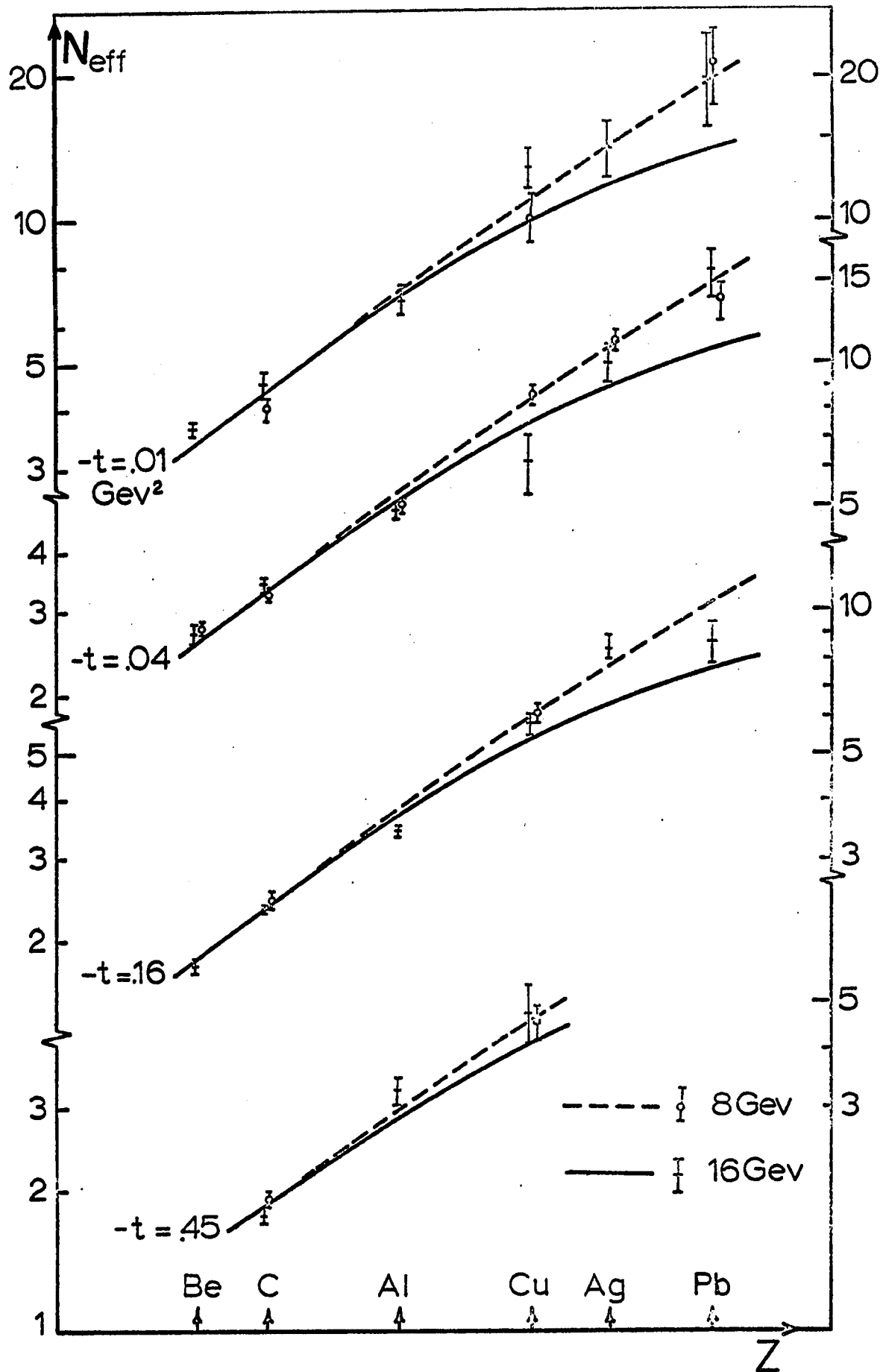
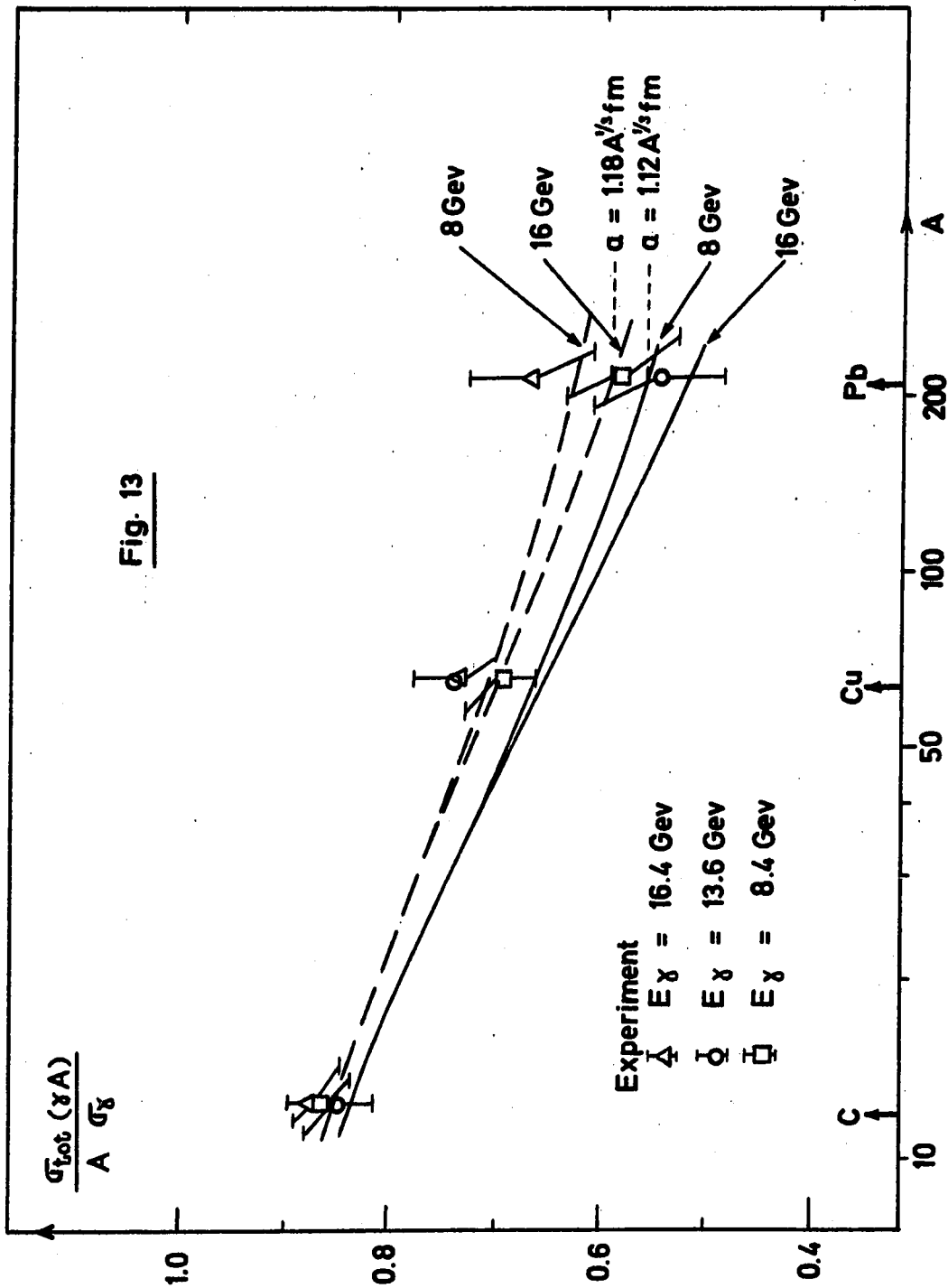


Fig. 12



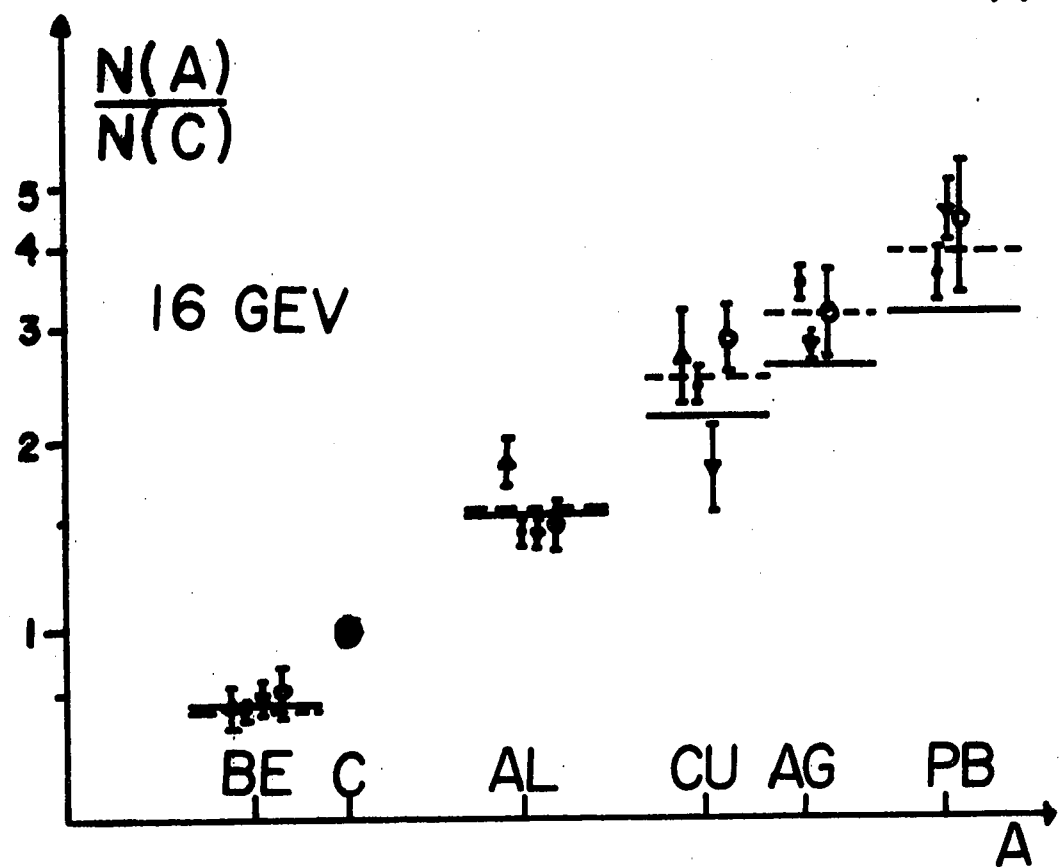
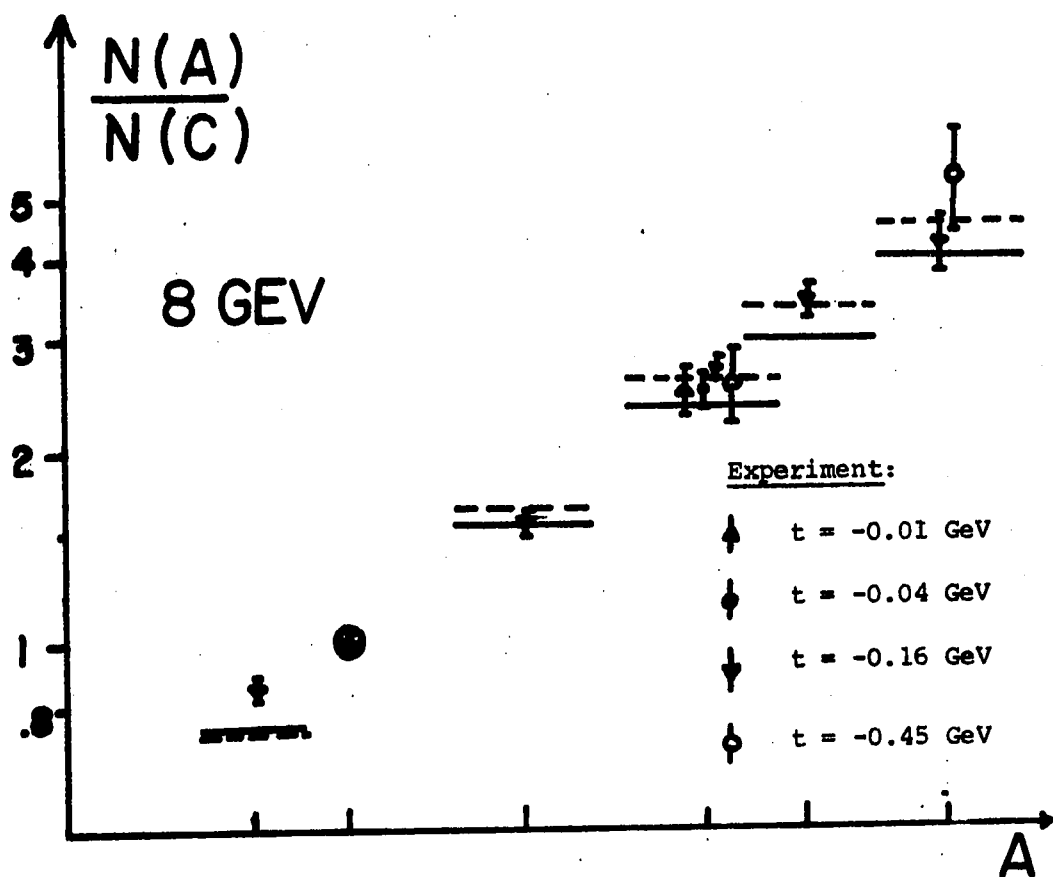


FIG. 14

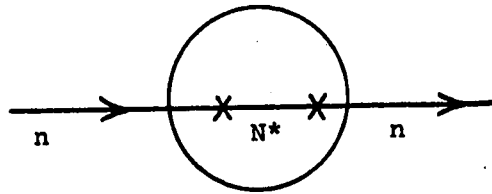
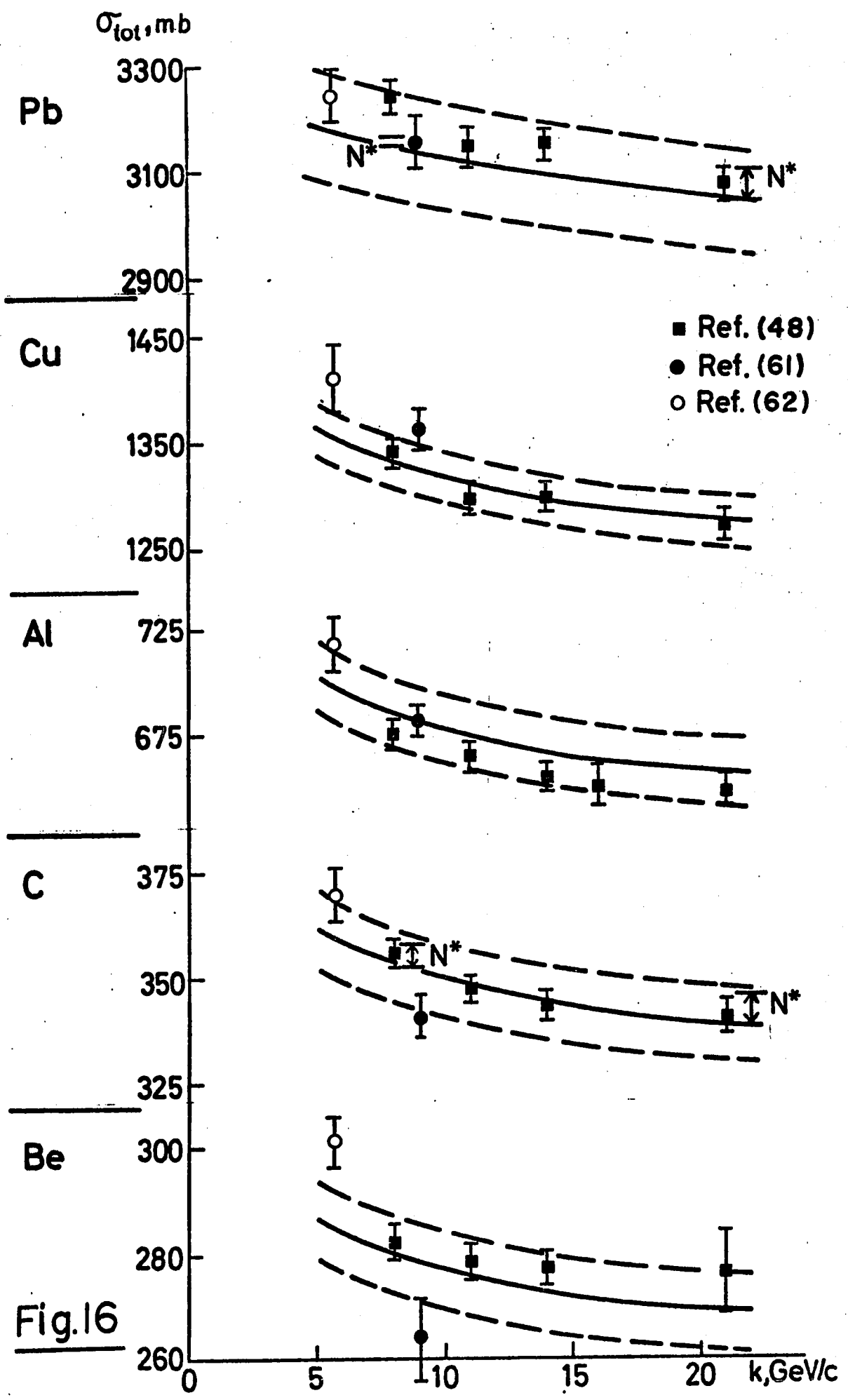


Fig. 15



A DEPENDENCE OF COHERENT PRODUCTION CROSS-SECTION
 $1 < M(\pi^+ \pi^- \pi^-) < 1.2 \text{ GeV}$

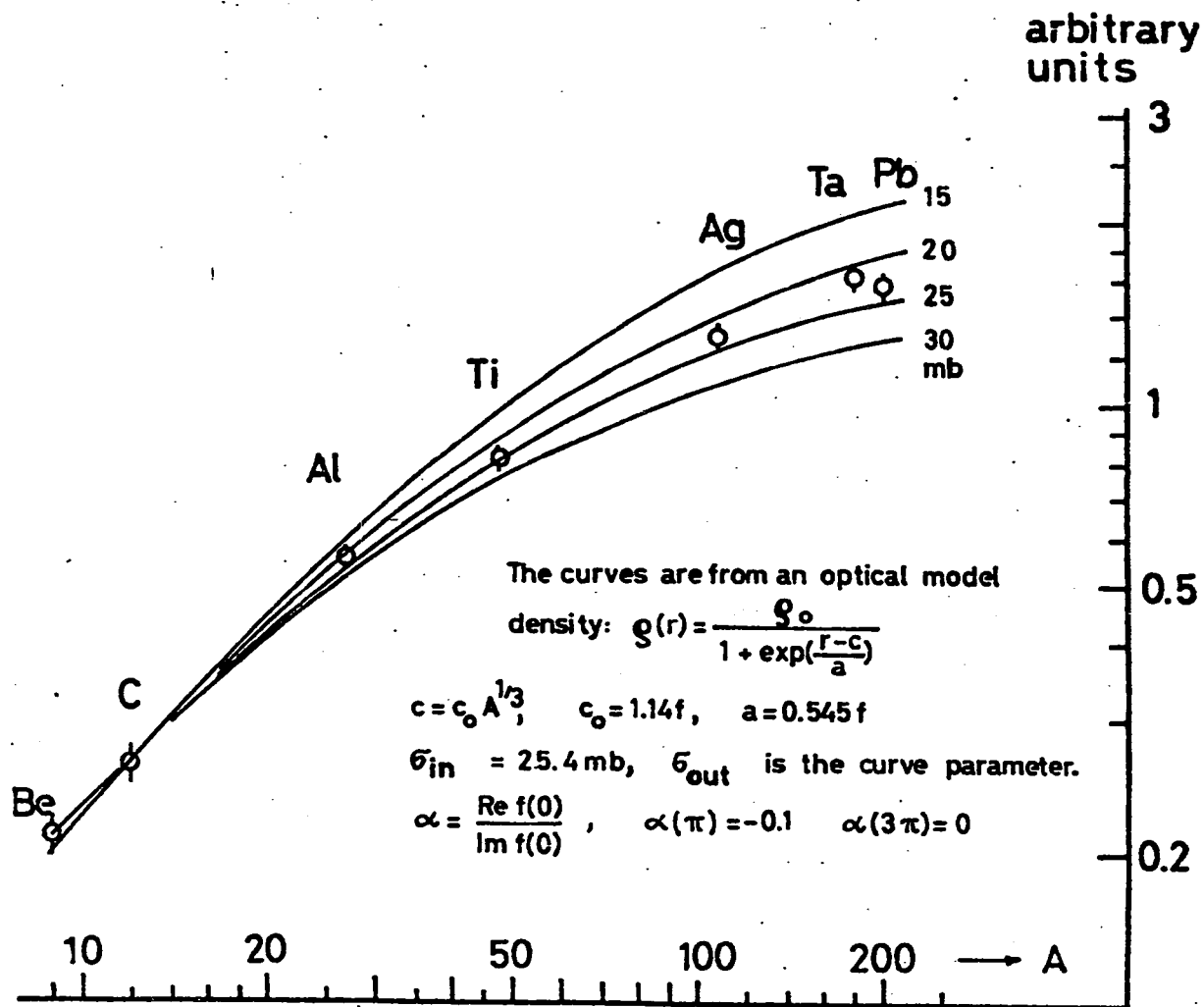


Fig. 17